AD-A050 878 BRITISH COLUMBIA UNIV VANCOUVER INST OF OCEANOGRAPHY F/G 14/2
TURBULENT VELOCITY MEASUREMENT WITH AN AIRFOIL PROBE,(U)
OCT 77 T R OSBORN, W R CRAWFORD N00014-76-C-0446
UNCLASSIFIED IOUBC-MS-31 NL

| OF |
AD
A050 878

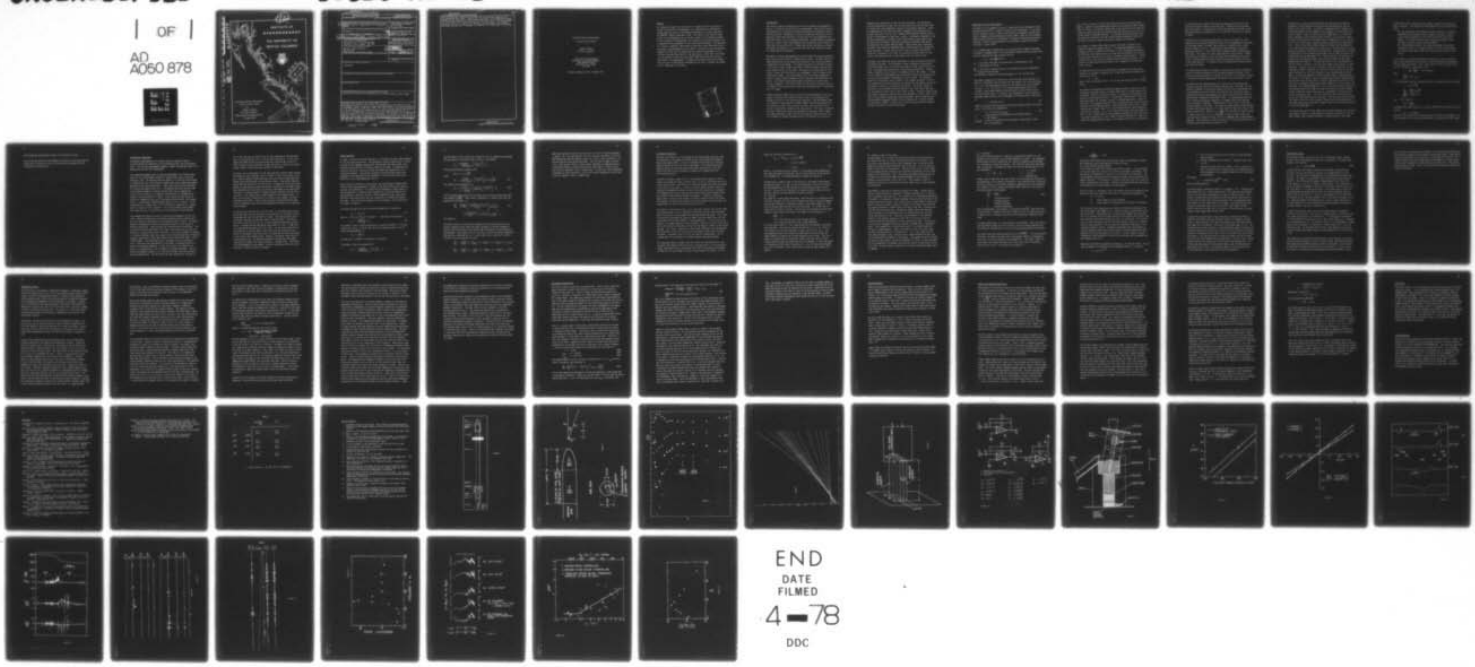

END
DATE
FILMED
4-78
DDC

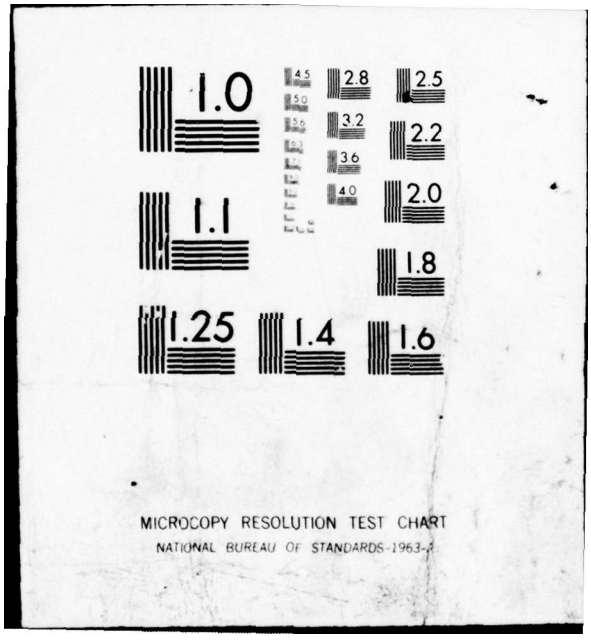
1.0
1.1
1.25
1.4
1.6
1.8
2.0
2.2
2.5
2.8
3.2
3.6
4.0
4.5
5.0
5.6
6.3
MICROCOPY RESOLUTION TEST CHART
NATIONAL BUREAU OF STANDARDS-1963-A

A2 SC

INSTITUTE OF OCEANOGRAPHY

THE UNIVERSITY OF BRITISH COLUMBIA

Turbulent Velocity Measurement with an Airfoil Probe

by

Thomas R Osborn

William R Crawford

IOUBC Manuscript Report No 31

October 1977

UNCLASSIFIED

SECURITY CLASSIFICATION OF THIS PAGE (When Data Entered)

REPORT DOCUMENTATION PAGE

READ INSTRUCTIONS BEFORE COMPLETING FORM

1. REPORT NUMBER

2. GOVT ACCESSION NO.

3. RECIPIENT'S CATALOG NUMBER

4. TITLE (and Subtitle)

(6) TURBULENT VELOCITY MEASUREMENT WITH AN AIRFOIL PROBE,

5. TYPE OF REPORT & PERIOD COVERED
IOUBC Manuscript Report
No. 31, 1977

6. PERFORMING ORG. REPORT NUMBER

7. AUTHOR(s)

T. R. Osborn and W. R. Crawford

(10) Thomas R. Osborn William R. Crawford

(15) 8. CONTRACT OR GRANT NUMBER(s)

N00014-76-C-0446 NR 083-207

9. PERFORMING ORGANIZATION NAME AND ADDRESS

Institute of Oceanography
The University of British Columbia
Vancouver, B.C., Canada V6T 1W5

10. PROGRAM ELEMENT, PROJECT, TASK AREA & WORK UNIT NUMBERS

(14) IOUBC-MS-31

11. CONTROLLING OFFICE NAME AND ADDRESS

Office of Naval Research
ONR Code 481
NSTL Station, Mississippi 39529

(11) 12. REPORT DATE

Oct 1977

13. NUMBER OF PAGES

56 pp (12) 61 P.

14. MONITORING AGENCY NAME & ADDRESS (if different from Controlling Office)

15. SECURITY CLASS (of this report)

15a. DECLASSIFICATION/DOWNGRADING SCHEDULE

16. DISTRIBUTION STATEMENT (of this Report)

Unlimited

17. DISTRIBUTION STATEMENT (of the abstract entered in Block 20, if different from Report)

18. SUPPLEMENTARY NOTES

19. KEY WORDS (Continue on reverse side if necessary and identify by block number)

Velocity microstructure, dissipation rate, velocity probe, airfoil probe.

20. ABSTRACT (Continue on reverse side if necessary and identify by block number)

This Manuscript Report is the result of a request for a contribution to the NATO Advanced Study Institute on Instruments and Methods in Air-Sea Interaction in USTAOSET, Norway, 16-28 April 1978. The result is too long for publication in the proceedings and so we have issued it as a Manuscript Report of the Institute of Oceanography, The University of British Columbia, with a condensed version prepared for the conference proceedings. The objective is to have as complete a description as possible of the characteristics of the probe as we see them now, and to make it available to the oceanographic community so that they

...12

DD FORM 1 JAN 73 1473 EDITION OF 1 NOV 65 IS OBSOLETE
S/N 0102-LF-014-6601

UNCLASSIFIED

SECURITY CLASSIFICATION OF THIS PAGE (When Data Entered)

063770 JOB

can understand the system of measurement in use, and then interpret the results of the data taken. Along these lines there is also Manuscript Report No. 30 (October 1977) discussing the free-fall body used in the measurements. As you will notice in reading this Report, there are gaps in our present knowledge and the work in progress or needed to fill these gaps is outlined.

Turbulent Velocity Measurement

with an Airfoil Probe

Thomas R Osborn

William R Crawford

Institute of Oceanography
University of British Columbia
2075 Wesbrook Place
Vancouver, B C, Canada
V6T 1W5

Manuscript Report No 31 - October 1977

Preface

This Manuscript Report is the result of a request from Dr Russ Davis at Scripps Institution of Oceanography for a contribution to the NATO Advanced Study Institute on Instruments and Methods in Air-Sea Interaction in USTAOSET, Norway, 16-28 April 1978. The result is too long for publication in the proceedings and so we have issued it as a Manuscript Report of the Institute of Oceanography, the University of British Columbia, with a condensed version prepared for the conference proceedings. The objective of this report is to have as complete a description as possible of the characteristics of the probe as ~~we~~ see ~~them~~ now, and to make it available to the oceanographic community so that they can understand the system of measurement in use, and then interpret the results of the data taken. Along these lines there is also Manuscript Report No 30 (October 1977) discussing the free-fall body used in the measurements. As ~~you~~ will be noticed in reading this Report, there are gaps in ~~our~~ the present knowledge and the work in progress ~~or~~ needed to fill these gaps is outlined.

Introduction

The study of oceanic turbulence on the scale of tenths and hundredths of metres is limited by the difficulty of measurement. Small-scale velocity fluctuations are of interest for they demonstrate the presence of turbulence and mixing. Temperature, salinity and density fluctuations can be measured, albeit with difficulty, to the scale of a few centimetres and these data used to infer mixing and turbulence. Unfortunately, the measurements of a scalar field like temperature or salinity do not give much insight into the velocity field. Rather than belabor the point, we assume the reader to be aware of, if not familiar with, the literature on what is called ocean microstructure.

Atmospheric velocity measurements are usually made with heated anemometry, hot wires and films which are inherently non-linear. In water there are added problems due to the higher heat capacity of the fluid and plankton contamination of the probes. This paper discusses an alternative sensor - the airfoil probe - which has neither of those problems, and hence may prove simpler to use in the ocean. The probe is a pointed body of revolution in which the lift force on the axisymmetric nose is sensed with a piezoceramic sensor. The probe measures the cross-stream component of velocity, whereas heated anemometry usually measures the downstream component - two crossed wires being needed to measure one cross-stream velocity component. The original ideal for the airfoil probe was due to H S Ribner at the University of Toronto and developed there in conjunction with T E Siddon.

Siddon and Ribner (1965) gave an account of the development of the early probes in which the lift forces on small disks (1.8 mm diameter) and planform airfoils of the same area were measured. That development work is discussed in great detail by Siddon (1965). Rather than measure the lift forces on a small wing section, for their later work they use an airfoil of revolution instead of the wing section. This work is outlined by Siddon (1971) with a much more detailed discussion by Siddon (1969). That paper describes a small pressure and velocity sensor that was built in an attempt to correct measured pressure fluctuations for the error

induced by the interaction of the flow with the probe. The discussion provides considerable insight into the flow about the probe and the range of validity for the assumptions involved in the probe's operation. There are comparisons of the velocity probe's response to that measured with crossed, hot wires in an air jet. Siddon (1974) describes further modifications to the probes for their use in water. Any reader interested in the validity, operation, or possible uses of the airfoil probes should read the University of Toronto, Institute of Aerospace Technical Note No 88 and Report No 136 (Siddon 1965 and 1969). They contain much information and detail that cannot be reproduced here without essentially reproducing those two papers. Rather, what we will do now is briefly outline the theoretical response of an airfoil of revolution and then report on and discuss the characteristics of the probes as we know them to date.

Throughout this paper the reader should bear in mind the vehicle from which we operate the probe. The instrument is used to measure fluctuations in the current shear $\partial u/\partial z$, $\partial v/\partial z$ over the range of scales from 3 to 50 cm in order to estimate the local rate of viscous energy dissipation. Figure 1 shows a schematic of the free-fall instrument we call the 'Camel'. To date its fall speed has been between 40 and 55 cm/sec and for the following discussion can be considered independent of time or depth. The imperfect behaviour of the Camel, such as change in fall speed, vibration, or oscillation about the vertical direction, are ignored for the general discussion and covered in detail at the appropriate points. The airfoil probe, a thermistor and salinometer head are mounted at the lower end of the body. The instrument has been used on three major cruises: June-July, 1974, along the Atlantic Equatorial Undercurrent on the ATLANTIS II; March, 1975, on the Azores Fixed Acoustic Range; and, October-November, 1975, on the Fine and Microstructure Experiment (FAME) cruise arranged by Dr T Sanford of WHOI on board the R V KNORR. Several local cruises have been used for testing and data collection on local inlet waters.

Behaviour of a Lift Force Sensor

The probe is an axisymmetric airfoil of revolution (Fig 2) mounted so that the mean velocity ($\vec{V}$) is aligned with the axis of revolution. In our application the mean velocity is due to the free-fall instrument, on which the probe is mounted, sinking through the water column. Much of the literature about forces on airfoils of revolution is related to derigible and missile problems. Since our system operates in the subsonic range, the airship literature is more useful.

For a slender body of revolution in an inviscid flow of speed U and angle of attack α (assumed small), Allen and Perkins (1952) derive the cross force per unit length due to the *potential flow* as

$$f_P = (\tfrac{1}{2}\rho U^2)\frac{dA}{dx} \sin 2\alpha \qquad (1)$$

f_P is the cross force per unit length due to the potential flow,
ρ is the density of fluid,
$\frac{dA}{dx}$ is the rate of change in body cross-sectional area with longitudinal distance along the body.
This formula is correct to the second power in α for inviscid flow.

The authors compare this theoretical result with the force observed on a model of a derigible, and find that near the forward tip of the derigible, for $\alpha = 6°$, the measurements agree well with theory, and viscous effects are small. At $\alpha = 12°$ and $18°$, the theory underestimates the forces slightly. The forward portion of the derigible is very similar to the tip of the shear probe. If equation 1 is integrated along the length of the shear probe from the tip to where $\frac{dA}{dx}$ is 0, then the total cross force is

$$F = (\tfrac{1}{2}\rho U^2)A \sin 2\alpha \quad . \qquad (2)$$

There is a second cross-force which is due to viscosity and/or flow separation. This force can be modeled as

$$f' \simeq \rho U^2 \sin^2\alpha \cdot R \cdot C_{d\alpha=90°} \qquad (3)$$

f' is the force per unit length due to viscous effects,
R is the radius,
$C_{d\alpha=90°}$ is the lift coefficient for the body in flow normal to the axis of revolution.

This force is exerted all along the probe and not just at the tip where $\frac{dA}{dx} \neq 0$. However, the aforementioned studies on the derigible model suggest that this force is relatively unimportant at the front end of the body for angles of attack less than 18° because separation does not occur until aft of the station of maximum diameter. The increasing cross-sectional area, the large axial velocity, and the finite distance upstream to the end of the body, all tend to reduce the possible effects of separation.

The studies of Siddon (1965, 1969) suggest the probe's response to be linear for angles of attack below 15°. The measured dependence of the response on angle of attack as determined in the calibration procedure to be discussed, also appears to be in accord with the potential flow theory. The non-linear response of the probe is presently being examined. Further information will be available from detailed calibrations by Nowell, a re-analysis of some previous calibrations, and a comparison with the wind tunnel results.

The theoretical ability of the shear probe to measure the cross-stream velocity u is evident if equation (2) is rewritten using the double angle relation for sin 2α.

$$F = \rho A V u \tag{4}$$

where V and u are shown in Fig 2. It can be seen that the force is linear with u.

The problem of exceeding the maximum acceptable angle of attack for linear response of the probe arises in regions where there is large current shear with depth. Shears as high as 60 cm/sec in 10 metres are reported at the Equator by Bruce and Katz (1976). Calculations indicate that if the four-metre-long Camel fell through a region of constant mean shear, a point on the body 1.5 to 2 metres above the probe tip would have the same horizontal velocity as the surrounding water. Using the maximum shear value of Bruce and Katz and a length scale of 2 m, the probe would see a mean horizontal velocity of 12 cm/sec. For a fall speed of 43 cm/sec, that corresponds to 15.6°. Such a large angle of attack probably exceeds the linear region for our present probes and is into a region of higher sensitivity. Hence the probe will overestimate the shear. The simplest solution to the problem is

to increase the fall speed of the vehicle assuming the position of zero relative horizontal velocity stays the same. Tipping of the instrument from the vertical is limited by the large righting moment inherent in the weight and buoyancy distribution to 1° or less with a period of 5 seconds or longer.

Calibrations of the present probes appear linear to at least 10°, with departures from linearity appearing at 12½° or 15° (depending on the probe). At the higher angles of attack the sensitivity increases with α faster than the factor of sin 2α. An appropriate and operational system for measuring the mean α is the device used by Simpson (1972) to measure the mean shear. His probe is in fact a mean angle of attack sensor. Comparison with data collected by that instrument on the Bermuda cruise may be useful in determining the possibility of excessive mean angles of attack in the Camel data set. At present we have no mechanism for monitoring the mean angle of attack.

For manufacturing reasons, the probes we have been using have an extensive region of constant diameter aft of the nose and before the metal sting. Since there could possibly be an effect of the flow in this region, a model of the probe has been manufactured and tested in the wind tunnel at UBC.

The model probe was manufactured out of plastic with 16 pressure taps located at various radii and distances from the nose. The model was four times the diameter of the oceanic probes with the outline determined from an enlargement of the drill which cuts the mold for the oceanic probes. Pressure distribution measurements were taken in the small wind tunnel of the Mechanical Engineering Department of UBC. The measurements were made with a pressure transducer connected to a computer-controlled stepping valve and digital voltmeter. Determination of $\frac{1}{2}\rho U_\infty^2$ is by a Pitot tube mounted adjacent to the model. The Reynolds number based on probe diameter and mean free stream speed was 2.5×10^4, about 10 times the value for the oceanic application. Values of $C_p = \frac{P-P_\infty}{\frac{1}{2}\rho U_\infty^2}$ were recorded for nominal angles of attack from 0° to 18° in 3° increments in the horizontal plane, the probe was then rotated 15° about its axis of symmetry and the measurements repeated. The resolution in angle of attack is 3° and the resolution of the pressure distribution about the probe is 15°.

The values of C_p can be used to determine the horizontal and vertical components of the transverse force using the probe dimensions and the slope of the probe surface. The slope is determined from a computer fit to the measurements of the diameter at the position of the pressure ports along the probe. Figure 3 shows the plots of $\frac{dL_H}{dx}$ where L_H is the horizontal component of the transverse force versus x for the various angles of attack. Note that the first panel which is nominally 0° has a non-zero lift; in fact, the analysis shows the angle of attack to have been about -1.8°. Thus all the other values of angle of attack must be reduced by 1.8° since the relative angles are accurate to .1° and the offset is in the original alignment of the probe to the mean flow. Examination of the vertical component of the transverse force shows that the model probe was also tipped slightly nose-down about 1.8°. During analysis, one pressure port was found to have been defective so the data from that port have been deleted from the analysis. The positions on the x-axis corresponding to the two lengths of probes in use have been marked on the figures for easy reference. Pressure ports were included to study the region aft of the long oceanic probe. Separation of the flow is quite visible at the high angles of attack for the later stations on the straight portion of the model. Careful measurements of the probe model show a slight decrease in the radius of the probe at the joint between the constant diameter section and the nose piece (Arthur Nowell, personal communications) and this discontinuity in diameter might induce vortex separation to occur sooner than otherwise. By integrating $\frac{dL}{dx}$ from 0 to x_i, one can study the variation of the transverse force with angle of attack for probes of varying lengths. Figure 4 shows the results where each x_i corresponds to the position of one of the pressure ports. Note the increasing slope to the lift force curve with increasing length of the probe. Even near zero angle of attack the slope of the lift curve increases slightly with increasing length of the probe even when the increasing length is due to the cylindrical portion of the probe where $\frac{dA}{dx} = 0$.

For the pressure ports in the region of increasing diameter, the variation with angle of attack is linear within the accuracy of the data. For the probe length, that includes substantial straight sections, non-linear

contributions to the transverse force become apparent as the angle of attack increases. From these data there appear to be two useful conclusions:

(1) The transverse force depends on angle of attack in a manner determined by the shape and total length of the probe. There is a non-linear contribution to the lift force due to the viscous effects. The results indicate that reducing the length of the cylindrical section reduces the non-linearity.

(2) The cylindrical part of the probe contributes to the total transverse force at all angles of attack in a non-trivial fashion. This result gives some insight into the question of spatial resolution.

At this point it is worth estimating the variation in angle of attack that is associated with the turbulence velocity fluctuations responsible for the energy dissipation. For a large value of the dissipation rate ε, say 10^{-2} cm^2/sec^3, in an isotropic field

$$\varepsilon = \frac{15}{2} \nu \overline{\left(\frac{\partial u}{\partial z}\right)^2} = 10^{-2} \text{ cm}^2/\text{sec}^3$$

then

$$\overline{\left(\frac{\partial u}{\partial z}\right)^2} \sim 10^{-1} \text{ sec}^{-2}$$

If the turbulent velocity fluctuations were a sinusoidal function of depth

$$U = U_o \sin \frac{2\pi z}{\lambda}$$

$$\frac{\partial u}{\partial z} = \frac{2\pi U_o}{\lambda} \cos \frac{2\pi z}{\lambda}$$

$$\overline{\left(\frac{\partial u}{\partial z}\right)^2} = \frac{4\pi^2 U_o^2}{\lambda^2} \cdot \frac{1}{2}$$

for $\varepsilon = 10^{-2}$ cm^2/sec^2

$$U_o^2 = \frac{\lambda 2}{20\pi 2}$$

An excessively large value of λ for such a high dissipation would be 10 cm, giving

$$U_o = .7 \text{ cm/sec}$$

and for a fall speed of 50 cm/sec the angle of attack varies between $\pm$ .8°. The turbulence is of course more peaked than a sinusoidal, but the length

scale chosen was deliberately chosen to be excessively large.

Thus, while the sensitivity may depend non-linearly on the mean angle of attack, the variation of α due to the small-scale turbulent velocity fluctuations is quite small.

Construction Techniques

The general requirements for an oceanic velocity sensor are that it (1) have sufficient sensitivity, (2) be pressure proof, and (3) be waterproof. The last two requirements suggest a robust construction that is incompatible with the first requirement.

The transducing element used to sense the aerodynamic lift force on the probe tip is a piezoceramic crystal of length 13 mm, width 1.6 mm, and thickness .5 mm. As received from the supplier, it consists of two layers of piezoceramic with a thin metallic center layer and a conductive surface deposited on the two outside faces. These faces form the two electrodes for sensing the output (see Fig 5). The applied force puts the top side of the sensing element in tension and the lower side in compression. Since the two crystals are of opposite polarization the voltages add to produce a non-zero output of voltage. Axial forces put both halves in tension or compression and, due to the opposite polarization, the outputs cancel. A piezoceramic bending moment sensor is an a.c. device. It can be modelled as a voltage source in a series with a capacitor or a charge source in parallel with a capacitor. We find the voltage source model more useful and use it exclusively for the electronic circuit analysis.

Two perpendicular beams are used to sense the two components of the lift force. They are glued with a five-minute hard epoxy onto a square brass pin while held at right angles by a jig machined out of teflon. The actual degree of orthogonality cannot be determined visually by any system to which we have access. Hence we check this feature during calibration. The two faces of the two beams which are glued to the brass post are then connected to it electrically with silver paint. The entire assembly is mounted in a hollow stainless steel tube, epoxy filled from the back end for pressure proofing, and finally a nose piece molded on with PRC 1201-Q (Med), a polysulfide rubber. The nose material has a hardness of 40 on the Shore A scale. There are four requirements on the epoxy, or whatever material is used for the sealing compound: it must be (1) soft; (2) impervious to water; (3) incompressible; and (4) adhere to adjacent materials. The construction procedure requires it to flow well through restricted passages and to be bubble-free. The PRC 1201-Q has been selected for its ease of

use in that the nose is bubble-free, has good adhesions to the stainless steel for waterproofing, and is soft to allow sensitivity. In this last regard the material must be stiff enough not to deform due to the lift force, but be as soft as possible so that the force is taken by the piezoceramic element and not the epoxy adjacent to the beams.

The actual tip on the probe is 19 mm long from the stainless steel forward. The change in cross-sectional area is limited to the 7.5 mm region at the end. Shorter probes (14 mm) have been built by inserting the probe sting further into the mold when casting the nose piece. They exhibit approximately 20% less sensitivity in calibration. We made the first short probe because of some questions about the spatial averaging of the longer probes. Upon examining the short probe, we noticed a shrinkage of the epoxy which resulted in an abrupt change in diameter between the epoxy and the stainless steel. This effect had not been apparent on the longer probes. In order to avoid this problem we will try some silicon rubbers with lower shrinkage coefficients. Oakey (1977) discusses construction techniques used at the Bedford Institute of Oceanography for making single component airfoil probes.

A problem arose from the use of silver paint in the construction process. Due to the small size of the probe it was possible for the paint to flow undetected and short out one-half of a beam. Even when examined under a microscope, the path of the short cannot always be found. The effect, once one is alert to look for it, is easily detected by measuring capacitance. A normal beam has 600-800 pf capacitance at 1 kHz. A beam with one side shorted has about twice that value. As the later discussion of the electronic circuitry shows, this effect does not change the sensitivity of the beam to the cross-force, for doubling the capacitance makes up for halving the voltage output. However, the thermal shock effect is significantly worse. We found the problem by looking for some common characteristic probes with large responses to thermal shock. Sufficient care and knowledge of the problem - we check capacitance after the paint has dried - serve to avoid this problem.

Signal Handling

In order to discuss the probe behaviour it is necessary to have some knowledge of the associated electronics. The electronic circuits before July 12, 1974, utilized a high impedance preamplifier located near the shear probe, and a differentiating amplifier in the main body of the Camel. Calibrations performed on the early calibrator allowed the probe and preamplifier to be calibrated together. The present calibrator to be described shortly was completed at the beginning of the ATLANTIS II cruise and required a preamplifier to be wired permanently into it.

During free-fall profiles at the equator, the low-frequency thermal sensitivity of the probe generated a voltage in the probe sufficiently large to saturate the preamplifier. To reduce the low-frequency voltage output of the preamplifier, a differentiating preamplifier was constructed for use during free-fall profiles (called a field preamplifier) and a band pass amplifier with uniform gain over the frequencies of interest was used in the Camel. The calibration preamplifier was unchanged. The circuits are all shown in Figure 6.

The output voltage from the calibration preamplifier is defined as

$$V_{C1} = \tfrac{1}{2}\rho S_1 \cdot Vu_1 \tag{5}$$

where S_1 is the sensitivity of channel 1. From the circuit analysis

$$V_{C1} = \frac{-j\omega C_p R_1}{1+j\omega C_{1C} R_1} \cdot V_i \tag{6}$$

for channel 1, and a similar expression is valid for channel 2. From the values of R_1 and C_1 it can be seen that for frequencies above 1 Hz, an excellent approximation is

$$V_{C1} = \frac{-C_p}{C_{1C}} \cdot V_i \tag{7}$$

and the gain is uniform at frequencies of interest.

The output of the field preamplifier

$$V_{F1} = \frac{-j\omega R_{IF} C_p}{(1+j\omega R_{IF} C_{1C})} \left[\frac{R_5 + R_6}{R_5}\right] V_i \tag{8}$$

and the output of the calibration preamplifier may be combined to eliminate the capacitance of the shear probe C_p which is an unknown.

$$V_{F1} = \frac{-j\omega R_{IF}C_{IC}}{(1+j\omega R_{IF}C_{IF})} \left[\frac{R_5 + R_6}{R_5} \right] V_{C1}$$

Using the derivative of equation (5)

$$j\omega V_{C1} = \tfrac{1}{2}\rho S_1 V \frac{\partial u}{\partial t}$$

gives

$$V_{F1} = \frac{R_{IF}C_{IC}}{(1+j\ R_{IF}C_{IC})} \left[\frac{R_5 + R_6}{R_5} \right] \left[\tfrac{1}{2}\rho S_1 V \right] \frac{\partial u}{\partial t}1 \qquad (9)$$

The response of the amplifier is

$$V_{A1} = \left[\frac{-1/R_2}{1+\frac{1}{j\omega R_2 C_2}} \right] \left[\frac{R_3}{1+j\omega R_3 C_3} \right] \left[\frac{R_7 + R_8}{R_8} \right] V_{F1} \qquad (10)$$

The FM telemetering system from the Camel to the surface system steps down the voltage by $\frac{1.414}{2.5}$. When Taylor's hypothesis is invoked, the final expression for the shear is

$$\frac{\partial u_1}{\partial x_3} = \left[\frac{2.5}{1.414} \right] \left[\frac{(1+\frac{1}{j\omega R_2 C_2})(1+j\omega R_3 C_3)}{-R_3/R_2} \right] \left[\frac{R_8}{R_7 + R_8} \right] \qquad (11)$$

$$\times \left[\frac{1 + j\omega R_{IF}C_{IF}}{R_{IF}C_{IC}} \right] \left[\frac{R_5}{R_5 + R_6} \right] \left[\frac{1}{\tfrac{1}{2}\rho S_1 V^2} \right] V_i$$

for channel 1.

The three circuits in use now (two preamplifiers and the amplifier) were tested by measuring the input and output voltages at various frequencies and by a white noise test utilizing the PDP-12 computer at the Institute of Oceanography. Each channel of each individual circuit was tested separately; the probe was simulated by an a c power supply and a capacitor in series. The best fit of the results is given

$$\frac{\partial u_1}{\partial x_3} = \frac{-1.80}{\rho S_1 V^2} \left(1 + \frac{1}{.17j\omega} \right) (1 + .0022j\omega) (1 + .0031j\omega) V_i \qquad (12a)$$

$$\frac{\partial u_2}{\partial x_3} = \frac{-1.75}{\rho S_2 V^2} \left(1 + \frac{1}{.17j\omega} \right) (1 + .0024j\omega) (1 + .0025j\omega) V_2 \qquad (12b)$$

where the constants 1.80 and 1.75 have units of (sec^{-1}), and are accurate to about ± 5%. The low-frequency roll-off, given by the ratio $1/.17j\omega$ has been determined from the nominal values of R_2 and C_2, each accurate to ± 5% and not from the tests described above. This roll-off is about -3 db at 1 Hz. The low pass filters in each channel combined to attenuate the differentiated signals as double pole filters, half power (-3 db) at 30 Hz and 33 Hz for channels 1 and 2, respectively. In addition, the FM telemetry attenuates at high frequencies, and has half-power frequencies of 80 Hz and 60 Hz for channels 1 and 2, respectively.

Calibration Technique

Two water flow devices for calibration of the shear probes have been used. One operates at flow speeds of 100-150 cm/sec, and has been described by Osborn and Siddon (1975). A flow is directed at the probe by a rotating nozzle inclined at 5° to the axis of the probe. This calibration device operates poorly at flow rates below 100 cm/sec and rotation rates less than 16 Hz; and it gives no check of linearity of response with the cross-stream velocity.

A second calibrator, shown in Fig 7, incorporates major changes to allow slower flow speeds and lower rotation rates. A jet is discharged vertically into a tank of water, with the tip of the probe mounted just above the center of the outlet at an angle α. Water for the jet passes through a mesh and honeycomb arrangement to reduce the scale size and intensity of turbulence The honeycomb also reduces large-scale vorticity which would produce disastrous effects when advected through the reducer. A design of Smith and Wang (1944) is used for the reducer to create a uniform flow at the nozzle. The diameters at the wide and nozzle ends of the reducer are 10 cm and 2 cm, respectively, to give an area reduction ratio of 25.

The probe is tilted successively at 2½° intervals from 10° left to 10° right, and rotated about its axis, generating sinusoidal voltages from each beam which are carried to the preamplifiers mounted behind the probe. Slip rings bring positive and negative supply voltages from the preamplifier, and tap the signals from the two channels of the preamplifier. A fifth ring is for ground. The output signals are sent through a low pass (-3 db at 10 Hz) unity gain filter to an oscilloscope to check for any bumps or spikes in the output voltage. The filter is required to remove high-frequency noise generated by the vibrations of the slip rings and of the electric motor used to rotate the probe. A rotation rate of 2.5 Hz was used for calibrations. An increased rate of 5 Hz produced no change of output voltage magnitude.

The sinusoidal output voltages from the filters were measured with a true rms meter (Disa Model 55 D35) which was calibrated with a 2.5 Hz sinusoidal signal whose amplitude was determined with a well-calibrated oscilloscope. In terms of the rms voltage, the peak voltage output for channel 1 of the

probe and calibration preamplifier is

$$V_{C1} = \sqrt{2}\, V_{rms} = \tfrac{1}{2}\rho S_1 U^2 \frac{\sin 2\alpha}{2}$$
$$= \tfrac{1}{2}\rho S_1 U^2 \sin\alpha\cos\alpha$$
$$= \tfrac{1}{2}\rho S_1 V u \qquad (13)$$

where S_1 is the sensitivity of channel 1 of the probe, which depends not only upon the nature of the probe, but also upon the gain of the calibration preamplifier. A similar expression is found for channel 2.

On board ship, a pump is used to drive the jet, the water recirculated through the system. On land, an overflowing bucket on the roof of one of the Oceanography huts at UBC provides a uniform pressure head to drive the jet. The use of this calibrator to provide accurate values of sensitivities requires the consideration of several factors.

(a) Gravity

The probe tip is more dense than water. When the probe is rotated with the tank full of water, but with no jet flowing, the force of gravity downward on the probe produces a sinusoidal voltage at the output terminals. This force is present when the jet flows past the probe. It is 180° out of phase with the force of the jet. The ratio of the voltages from the probe caused by these forces at 40 cm/sec flow speed in the calibrator is

$$\left|\frac{Lj}{Lg}\right| \sim 3$$

Lj is the lift due to the jet (always upward),

Lg is the gravitational force (always downward).

The ratio varies with V^2. This large effect was not foreseen in building the calibrator. With the jet flowing the net lift is $Lj - Lg$. With no jet flowing, but the probe immersed in water, the net lift is Lg. The corresponding output rms voltages were measured at various angles and added together to produce the voltage expected from Lj alone. This procedure is satisfactory for sinusoidal signals, but any noise or stray signals generated would be added doubly by this method. As the flow speed is increased to 70-80 cm/sec, where $|Lj/Lg| \simeq 10$, the stray noise becomes much less troublesome. Most calibrations are done at these higher flow speeds.

(b) Boundary layer in the nozzle

It would appear at first that the flow speed through the nozzle would be the volume flow rate in cm^3/sec divided by the area of the nozzle. The flow rate can be measured easily, but a boundary layer in the nozzle may reduce the effective cross-sectional area of the flow. This area must be known to calculate the flow speed U. The sensitivity varies as the square of this speed, and the variance of the velocity fluctuations varies as the square of the sensitivity. Thus, the energy dissipation which we want to estimate from the velocity shear variance depends on the 4th power of effective cross-sectional area of the flow. Small boundary layers or bubbles on the walls of the nozzle can cause large errors in the estimates of dissipation.

Some method is required to accurately measure the speed. The most satisfactory solution found is to measure the dynamic pressure $\frac{1}{2}\rho U^2$ in the jet with a manometer and pitot tube. This system has the advantage of measuring U^2 directly. A large bore inclined manometer gives accurate readings of the height of the water column. For a pitot tube, a plastic pipet is used, with part of the tip cut away to leave a 4 mm end to be directed into the flow. The dynamic pressure is uniform across the core of the jet. Pressures outside the jet are uniform also. Abramovich (1963) states that observed static pressures in a submerged jet such as observed here are the same inside and outside the jet. Therefore, the difference in the pressure observed is the dynamic pressure of the flow in the core of the jet. Figure 8 shows the flow speed for various volume flow rates. The value of U^2 given by the manometer should be accurate to better than 1% (Bradshaw, 1964). The repeatability of results was within 2% to 4% and should be the error in measurements. There is no reason for the fit to be linear, but the line drawn does fit the points well. It is also noted that the flow speed increases slowly in time during a steady volume flow rate, due to an accumulation of bubbles in the nozzle. Flow speeds could be increased by 5% due to this effect. During the ATLANTIC II cruise, no check was made on this accumulation of bubbles, and resulting errors in sensitivity can be up to 10%. For more recent calibrations, the nozzle has been brushed clean of bubbles.

(c) Turbulence

The large-scale turbulence is reduced by using packing material in the bottom of the calibrator, and aluminum honeycomb or straws. The honeycomb, manufactured by Hexel Corporation, was 3 mm cell diameter and 50 mm deep. It is mounted 9 cm below the reducer. The inflow of water below the honeycomb is turbulent. The Reynolds number for the flow through each cell of the honeycomb is

$$Re = \frac{Ud}{\nu} = 64$$

U = 3 cm/sec
d = 0.3 cm
ν = 0.014 cm^2/sec

Laminar flow in each cell may occur, which is not the optimum situation for the generation of low intensity turbulence. The turbulent flow in each cell would be preferred, giving lower intensity turbulence beyond the honeycomb. For laminar cell flow, Lumley and McMahon (1967) predict for the decay of turbulence beyond the honeycomb

$$\frac{\overline{u'^2}}{U^2} \sim \frac{0.03}{x} d \qquad (14)$$

u' turbulent velocity
U average velocity
d honeycomb diameter
x distance downstream

From the honeycomb to the reducer is 30 diameters and $\frac{\overline{u'^2}}{U^2}$ should be 0.001 at the reducer. Pankhurst and Holder (1952) give $\overline{u'^2}$ as roughly constant in a reducer, and U^2 increases by $(25)^2$, pushing turbulent intensities even lower.

The shear probe itself is a good detector of turbulence. With jet flowing and the probe inclined at 10° to the flow, the rms voltage observed with the probe not rotating was 2% of the rms voltage observed during rotations.

The signal from the rotating probe varies as $\frac{U^2 \sin(20°)}{2}$. The non-rotating probe will not detect the mean cross flow because signals at frequencies less than 0.1 Hz are filtered by the preamplifier. The output signal will only contain the higher frequencies of cross flows, due to turbulence, which vary as $Vu' \sim Uu'$. The ratio of the signals is

$$\frac{Uu'}{U^2 \frac{\sin 20°}{2}} = 0.02$$

from which $\sqrt{\overline{u}^2}/U \sim 0.3\%$ which indicates low levels of turbulence at scales and frequencies which the probe and filters will pass.

(d) Water tunnel blockage effects

In the ocean the probe falls through the ocean at speed V. In the calibration tank an open jet of water 2 cm across is directed at the probe. The deflection of streamlines in the jet is not the same as in the ocean. The jet streamlines spread more easily around the probe, reducing the effective dynamic pressure. If the probe is inclined in the jet, the lift is not the same as experienced in the ocean. Pankhurst and Holder describe the following corrections for these effects for wind tunnels.

When an airfoil is introduced into a wind tunnel, the solid blockage at the mid-point along the length of the airfoil is conveniently expressed by

$$U_F = U_T(L+\varepsilon_s) \tag{15}$$

U_T tunnel speed far from the model,

U_F tunnel speed at the mid-point of the chord of the model.

For the case of the shear probe, one wishes to find the blockage near the tip of the probe, where $\frac{dA}{dx} \neq 0$ (i.e., where the probe is most sensitive to the cross-flow). One possible way to examine the blockage near the probe tip is to consider only the rubber portion of the probe as the airfoil, and the stainless steel tubing behind the probe as a solid wake. This distinction is rather arbitrary, and the resulting fineness ratio of 5 is higher than the value derived if only the sensitive portion of the probe is considered as being an airfoil. Pankhurst and holder have cited results of Lock and Johansen (1931) who found the effect of wake blockage small when compared to the solid blockage of an airfoil. In the absence of better information, this assumption is held to be valid here, and we proceed with the fineness ratio of 5.

Pankhurst and Holder have published values of ε_s for various flows. For an open axisymmetric jet blocked by an axisymmetric body, ε_s is given by

$$\varepsilon_s = \tau_N \lambda_A \left(\frac{A}{C}\right)^{3/2} \tag{16}$$

$\frac{A}{C}$ ratio of cross-sectional area of probe to cross-sectional area of nozzle.

τ_N constant characteristic of nozzle = -0.206 for open circular jet.

λ_A constant characteristics of airfoil. This is chosen as 5 which is the value for a Rankine Ovoid of fineness ratio 5, and corresponds to the assumed fineness ratio of the probe as noted above.

This gives

$$\varepsilon_s = (-0.206)(5)\left(\frac{1}{16}\right)^{3/2} \approx 0.02 \qquad (17)$$

which has been neglected.

The second tunnel interference effect is a change in lift. Pankhurst and Holder show that for a finite width airfoil in an open jet, the measured lift will be less than encountered in a flow of infinite extent. This effect is diminished at the forward and trailing ends of the airfoil, so for the case of the airfoil shear probe whose lift is concentrated near the forward tip, this effect may not be large. The corrections given by Pankhurst and Holder apply only to an airfoil whose length is much smaller than the jet width, and do not apply in the case where the probe length is much longer than the jet width.

To determine the magnitude of these two tunnel interference effects, a probe was calibrated using two different nozzles, of diameter 1.92 and 3.00 cm, and for similar flow speeds the outputs with the larger nozzle were about 4% to 5% greater. The ratio of the nozzle areas is .41. The blockage effect varies inversely as the three-halves power of the area of the nozzle (equation 16) and the lift effect varies inversely as the area (Pankhurst and Holder) and an upper limit of the total error due to these two effects in the smaller nozzle is found by assuming the sum of these two errors to vary inversely as the nozzle area. In such a case, for the smaller nozzle, this total error is 6% to 8% of the measured lift. All calibrations were done with the smaller nozzle, and no correction has been made for this error. The possible effect of this correction will be more apparent in the discussion on spatial resolution.

Probe Sensitivities

As the probe rotates in the jet, the lift on the probe remains constant but the lift on the individual beam varies sinusoidally. The peak output voltage is for channel 1:

$$V_{C1} = S_1(\tfrac{1}{2}\rho U^2)\frac{\sin 2\alpha}{2} \qquad (18)$$

In practice, the rms voltage is measured and the peak voltage derived. To find S_1 and S_2, the values of $V_{rms}/\rho U^2$ are plotted versus sin 2α as in Fig 9. The flow rate is measured easily by trapping the overflow from the tank. The speed $\overline{U}$ is determined from the flow rate and the graph in Figure 8. For this probe the output voltage appears to be linear with sin 2α beyond $\alpha = 2.5°$ but is higher at small angles. This deviation is due to non-perfect alignment of the axis of the probe with the axis of the jet, such that $\alpha = 0°$ cannot be achieved. The relative angle of the jet can be measured accurately (better than 0.2°) but the absolute angle, as shown in Fig 9, was out by 1°. That is, the reading at 10° to the right was actually at 11°, and the reading at 10° to the left was actually at 9°, etc. One would expect that because sin 2α is not a linear function of α at angles near 10°, an error would result from mislabelling the angles in this way; however, the error is small (<1%).

A larger error results from a tilt of the entire plane of inclination relative to the jet axis. This angle is checked before a calibration, but one cannot be sure that it is less than 1°. If the plane of inclination is tilted forward at an angle of say 1°, then a true angle of 1° is present for a nominal angle of 0°. The effect of this tilt is diminished at larger angles; the true angle is 2% larger for a nominal angle of 5°, 1% at 7½° and 0.5% at 10°. To calculate sensitivities, most weight was put on the values at these three higher angles, and the expected error in sensitivity is 2%.

The largest errors result from uncertainties in the flow rate in the calibrator during the ATLANTIS II cruise, and the tunnel interference effects. The probes were recalibrated upon our return to Vancouver, but variations of about 10% are found in the two sets of calibrations. It may be that the values of the sensitivities determined during the ATLANTIS II cruise

are up to 10% too high because of bubbles in the nozzle during the cruise, and 6-8% too low because of the tunnel interference effects. Other errors, such as uncertainties in the flow rate, in the angle of tilt and in the change of sensitivity with temperature may contribute to a lesser extent to the overall uncertainty in the value of the sensitivity. The overall error may be up to 20%. Errors in the probe sensitivities are smaller for recent calibrations.

Temperature Effects

The sensitivity of the probe is temperature dependent. Operational temperatures have ranged from as low as 4°C in the surface waters during the B C winter, to 26°C in the Equatorial Atlantic. Because of the complexity and the uncertainties of the calibration procedure, no detailed knowledge of the temperature dependency of the calibration is available. Several sets of calibrations have been performed at both ends of the operational temperature range and the results are consistent with a sensitivity change of +1%/C° of the sensitivity at 26°C. This factor is a few times larger than one would predict from the general temperature sensitivity of the piezoceramic material.

Fortunately, one does not encounter the entire temperature range in any given cruise and so judicious choice of the calibration temperature can limit the amount of correction required for a given set of data. Having said that, one must realize that calibrations in the winter are biased toward lower temperatures by the fact that the tap water in Vancouver is cold.

A more serious temperature-induced problem arises in the low-frequency voltages generated in the beams due to temperature changes. Figure 10a shows the voltage versus time plot for the output of the calibration preamplifier when a probe was moved from a cup of water at 15.1°C to a cup of water at 30.4°C and back again. The lower trace is the transition from hot to cold on an expanded time scale. There is a characteristic shape to the thermal response that is the same in both channels. The small amount of high-frequency variation at the start of the thermal response is due to the insertion of the probe into the cup of water and varies between the traces; the high speed trace (Fig 10b) is especially clean in this regard. The major response to heating is first toward negative voltage for a fraction of a second followed by a trend toward positive voltage, and then a decay back towards, but not to, the previous zero level. All probes show the same characteristic signature to the thermal response curve. There is one variation and that is that the curve can be inverted. Checking the directional response of probes with inverted thermal response shows them to have inverted output relative to the lift force, i.e. opposite beam

polarization. Thus, we conclude the thermal response curve is a characteristic of the beams and the way they are mounted in the probes for the signature of the curve can be predicted from the sign of the temperature change and the beam polarization.

While both channels show the same shape of response in Fig 10, the lower channel has an essentially positive voltage response to a temperature increase and the other channel has significant response of negative voltage as well as the positive voltage response. The negative voltage response is the quicker but the positive response lasts much longer. What would the Camel electronics show in this situation? For this discussion we can treat the frequency response characteristics of the calibrating preamplifier as being the same as the band pass amplifier in the Camel and say that the output of the Camel's shear circuits to a step change in temperature would be the same as the derivative of the curves shown in Fig 10. The derivatives of the two curves would not be as similar as the curves themselves; in fact, the maximum shears could well be of opposite sign.

At the southern edge of the Atlantic Equatorial Undercurrent the thermocline is quite sharp. Figure 11 shows a 10-metre span of data. The temperature difference is about 4.2°C between 52 m and 53 m depth. The probe's low-frequency thermal response is quite evident. The noise spikes marked with arrows are seen in some probes when exposed to thermal shock while some other probes never develop this problem. The spikes can be removed and the data points replaced but we retire probes as soon as possible after they show these spikes. The two channels display different responses, the second channel responding sooner but with less amplitude and in the opposite direction to the first channel. The response to the thermocline shown in Fig 11 is consistent with the response to a step change shown in Fig 8. Admittedly, it is difficult to compare the two traces for the step response must be convolved with the thermocline profile and then differentiated. The reader will note ch 2 of Fig 11 has a quicker time response to the start of the thermocline, but the net effect is only half as large. That situation is consistent with the upper trace of Fig 10a where the response is quicker

but the initial voltage swing is cancelled by the later trend of opposite sign, whereas in the lower trace the response is essentially of one sign but delayed in time by the small deflection of the opposite sign at the start.

In looking for an explanation for the large low-frequency response of the probes to changes in the mean temperature there are several sources that can be examined. First is the pyroelectric effect of the beams themselves. Recall that the transducing elements are formed as a sandwich of two layers of piezoceramic material with opposite polarization (Fig 2). If the dimensions of the two pieces are identical and the temperature change for each side the same, then the induced voltages should cancel. Clevite Corporation literature gives

$$\left(\frac{\partial p}{\partial \theta}\right)_{\text{stress}} \cong -2 \times 10^{-8} \text{ coulombs/cm}^2/\text{C}^\circ$$

where p is the polarization for one side of beams

$$\Delta V \simeq \frac{\Delta p}{C} = \frac{-2\text{x}10^{-8} \text{ coul/cm}^2/\text{C}^\circ(.18\text{cm}^2)}{1400\text{x}10^{-12} \text{ farads}}$$

$$\cong 2.6\text{volts/C}^\circ = 39\text{volts/15C}^\circ$$

So, the response in Fig 9 is a small fraction of the voltage change in each half of the beam and could result from a slight mismatch of the dimensions of the two halves or of the rate of heating. The beams are formed by sawing up a large plate of material that was created by bonding two layers on opposite sides of a metal substrate. Thus, there is no reason to expect the two layers in the beam to have the same thickness (i.e., the same capacitance). The two-beam probe that we use is inherently axymmetric with one side of the beam closer to the edge of the probe than the other (see Fig 2). Thus the temperature change affects one side before the other, possibly imposing a mechanical strain in addition to the direct induced temperature effect. This mechanical strain can in turn cause a voltage output. A poor choice of substrate or epoxy can induce further strain by differential thermal expansion.

Further tests are needed on the beams themselves to better judge what is happening. We have purchased some specially made beams from Gulton

Industries in the hopes that close matching of the two halves will reduce the net pyroelectric effect and that their choice of epoxy and center substrate will reduce the differential heating problem. We plan on testing the beams alone to determine how much of this effect is inherent in the transducer itself and what portion is due to the configuration of the probe.

Turn now to the question of the high-frequency response of the probes to temperature fluctuations. Are the signals that we interpret as velocity fluctuations contaminated by the high frequency temperature fluctuations? Figure 12, which is data from 28°01'W, 0°18'S, shows a large temperature change just above 70 metres depth with several small-scale temperature gradient fluctuations associated with it, yet no corresponding small-scale velocity shear fluctuations. The mean response to the net temperature change is visible. This temperature features is interesting. It appears to be close to the depth of the salt core in the undercurrent. Several of these features have been observed by various temperature microstructure instruments at UBC (Laurent Bilodeau, personal communication). They are distinctive by their one-sided gradient profile, since the temperature gradient does not change sign, they may not be turbulent but rather a manifestation of the convection associated with double diffusive processes. They appear to occur in regions where we never have sufficient data to unequivocally rule out the likelihood of salt fingering. There must be some source of motion to produce the fluctuations in temperature gradient shown. However, horizontal velocities do not seem to be the source. For assessing the possible effect of small-scale temperature effects, it is very useful to have such a large temperature change with no associated velocity fluctuations. Figure 13 shows some data collected on the Azores Fixed Acoustic Range. The temperature and temperature gradient traces both show a well-mixed region between 110 m and 155 m, but the velocity shears show the turbulent region to be nearly continuous through this region. Here we see velocity fluctuations without any associated temperature fluctuations, presumably because the fluid is well mixed and the temperature inhomogeneities have all been dissipated by thermal diffusion. (Note that the full-scale values of the shear are 10 times those of Fig 12.) Figure 1 of Osborn and Siddon (1975) showed velocity fluctuations and the associated temperature fluctuations for the different patches over 60 m depth intervals. There

the temperature fluctuation's intensity appeared to be inversely correlated to the velocity fluctuations unless one accounted for the variation with depth of the mean temperature gradient.

Considering the effort necessary to get temperature sensors with reasonable thermal response it is unlikely that the velocity probes, being much larger than the thermistors generally used and with their construction of insulating rubber, can respond at the high frequencies associated with the temperature gradient fluctuations. The most likely source of trouble is with the spiking observed in Fig 11. Big spikes are obvious but a bad probe can also generate small spikes. Experience generally assists one to tell good data from bad. The spikes in Fig 10 at 75.5, 79.5 and 82 metres are considered to be faulty data because of their asymmetric shape and lack of associated temperature gradient fluctuations. The data at 65 m are accepted because of the association between temperature and velocity fluctuations. The velocity shear spike at 72 m is suspect because of its isolation although it could possibly be real. There are considerably fewer problems with spikes in the Azores data than the Equatorial Undercurrent data, perhaps because the Azores data were all taken with one apparently excellent velocity probe (15 drops).

Acceleration Sensitivity

The airfoil probe is sensitive to accelerations. Being a force sensor the probe interprets a lateral acceleration as a force due to the inertial loading of the probe tip. Figure 14 shows the acceleration sensitivity $S_g(f)$ as a function of frequency of a short-nosed airfoil probe as measured on a shaker table. The output was measured with electronics equivalent to that in the Camel except for telemetry and is given in millivolts per milli-g. These data were provided by A Nowell of the Ocean Mixing Group at Victoria, B C. He also indicated that the output ratio was independent of the magnitude for the acceleration as determined by varying the amplitude of the vibration at selected frequencies from 50 milli-g's to 250 milli-g's. These data are for a probe vibrated in air. In water the added mass effect (Lamb 1945) should not double the output since the probe tip is denser than water and the added mass is less than the displaced volume of water.

There is a second aspect to the probe's acceleration sensitivity and that is due to the fact that a vibrating probe sees a varying angle of attack of the mean veloctiy vector. Thus even a set of crossed wires which have no acceleration sensitivity, when vibrated perpendicular to a steady flow, would respond as if they were in a time-varying cross-flow. Similarly, a hot film vibrated in the down-stream direction senses the apparent fluctuation in the flow. Suppose an airfoil probe is vibrated back and forth perpendicular to the mean flow with an amplitude ℓ and a radian frequency ω. We can calculate the velocity and acceleration of the probe tip.

$$x = \ell \sin \omega t \tag{19a}$$

$$V_{tip} = \dot{x} = \omega \ell \cos \omega t \tag{19b}$$

$$a_{tip} = \ddot{x} = -\omega^2 \ell \sin \omega t \tag{19c}$$

The apparent water velocity as seen by the probe tip is $u = -v_{tip}$ and the shear as sensed by the instrument is

$$\frac{\partial u}{\partial z} = \frac{\partial u}{\partial t} \Big/ \partial z/\partial t = \frac{\partial(-v_{tip})}{\partial t} \Big/ v_{fall} = \frac{-a_{tip}}{v_{fall}} \tag{20}$$

Let us now compare the magnitude of the two contributions to the output due to the probe's vibration. Assume for the data shown in Fig 14 that the probe sensitivity was $S \sim 3.5 \times 10^{-4}$ volts/dyne cm^2, and v_{fall} = 50 cm/sec, the

voltage output of the probe due to the apparent velocity of the water is:

$$V_{apparent} = \frac{\rho S v^2_{fall}}{-1.8\ sec^{-1}} \cdot \frac{-a_{tip}}{v_{fall}} = \rho S v_{fall} \cdot a_{tip}$$

$$\frac{V_{apparent}}{a_{tip}} = 17.5 \text{ millivolts/milli-g} \qquad (21)$$

Thus, for frequencies below the peak of the curve of the acceleration sensitivity shown in Fig 14, the major contribution to the output voltage is not due to the inertial loading effect but rather inherent in the fact that it measures the cross-stream velocity. Above that peak the problem of frequency response and spatial resolution (to be discussed later) limit the above discussion which is based on steady-state rather than a time-dependent response. Crossed wires would have almost as much noise due to a vibration at the low frequencies (less than 20 Hz). While a hot film probe suffers a similar contamination due to vibrations parallel to the direction of the mean flow, it is much less sensitive to cross-stream vibrations.

Figure 15 from Crawford (1976) shows a series of spectra from two-metre vertical sections of data. The dissipations have been estimated from the variance of the shear signal. Note how the high frequency portion of the spectrum has a consistent shape independent of the calculated dissipation. This region contains the vibrations and the electronic noise, the turbulence signal is at the lower frequencies, generally below 30 Hz. Especially noticeable is the vibration peak at 23 Hz. The instrument was built so that the vibrations would be out of the frequency band of interest (we got rid of most of the 23 Hz noise eventually) because it is impossible to build something that does not vibrate a bit at some frequency. From looking at our data, a reasonable estimate for the amplitude would be 10^{-3} cm. At a frequency of 30 Hz the associated velocity from equation (19b) is 2 mm/sec and the acceleration is about 40 milli-g's. Clearly the apparent velocity does not cause any problem with respect to the maximum angle of attack limitations, nor does the amplitude cause any problems with respect to moving the probe any sizeable fraction of its diameter and thus changing the potential flow characteristics. However, the amplitude is comparable to the boundary layer thickness on a sphere of this same diameter in a flow of the same speed. Since the amplitude is small the potential flow won't be affected unless there is separation or 'stalling' to modify the

flow. Fortunately, axisymmetric bodies are not prone to sudden changes in the slope of the lift curve until the angle of attack approaches 45°, well above the region we want for operation of the probe. Separation occurs at much lower angles in the form of a pair of vortices which are fed by vortex filaments originating at the separation lines (Nielsen 1960). As with a delta wing airplane, breakdown of this system and loss of lift do not occur until high angles of attack.

Pressure Effects

There are two possible effects one must consider; pressure induced noise, and a change in sensitivity with pressure. There is a noise spike that occurs intermittently on our velocity shear data records; we call it a 'boing'. It is one second long and has the form of an exponentially damped high-frequency oscillation. To determine the cause we tested a probe up in our pressure tank by itself and in conjunction with our Richardson-type stretched pin releases. The noise appears only when the probe is pressurized with the release. Keeping the releases and all other moving parts (the salinometer has several) greased has reduced the occurrence of these noise spikes.

We also tested the probe for a change in sensitivity with pressure by mounting a 12.7 mm diameter bar .3 m in front of the probe tip on the Camel. Drops were then made in excess of 200 m depth through isothermal water in Howe Sound (a local B C inlet). Preliminary analysis with an rms meter revealed no change in sensitivity over that depth interval to ± 5%. Analysis of the data shows a large fluctuation (± 20%) in the spectral level between 5-m intervals. When averaged over 50-m intervals, the spectral levels are constant to ± 2%, but the errors in fall speed make it impossible to determine if the sensitivity is constant to better than ± 5%.

Oakey (1977) has tested the pressure sensitivity by pressuring the probes in a chamber with a magnetic stirrer and looking at the rms output. He finds the sensitivity constant to better than ± 5% which is the estimated accuracy of the test.

Spatial and Temporal Resolution

Measurements of the velocity shear can be used to estimate the local rate of viscous energy dissipation. If one has all the necessary derivatives, the dissipation can be calculated exactly (Lamb 1945). Given the two terms we get from the Camel data, and using the relation for isotropic turbulence $\varepsilon = 7.5\nu\overline{\left(\frac{\partial u}{\partial z}\right)^2}$, one can estimate the dissipation. Osborn (1974) suggests that the value 7.5 could be replaced by 5 ± 2.5 to account for the distinct possibility that oceanic turbulence is not isotropic. However, it is probably better if the isotropic relation is used and people bear in mind the assumption of isotropy rather than to have different groups using different relationships to estimate the dissipation from their velocity gradient measurements. A crucial question is whether the variance of the velocity shear is completely resolved by the probe. Just as in the situation of estimating the turbulent heat flux from the small-scale temperature gradient, spatial averaging of the signals at the scale size of the peak of the spectrum can lead to seriously underestimating the variance.

There are actually two problems being studied at once, the spatial resolution problems in which a velocity fluctuation impinges on the probe with a varying value of the cross-stream velocity, modulating the angle of attack, at different positions on the probe. There is also a frequency response problem similar to the pitching airfoil (von Kármán and Sears 1938) in which the angle of attack is uniform but the flow is not in equilibrium with the instantaneous position of the airfoil. The response of the probe to any real feature will be a combination of the two effects.

Siddon (1969) compared the airfoil probe to a set of crossed hot wires in a jet. Unfortunately the intensity of the turbulence was too high for the behaviour of either the crossed wires or the airfoil probe to be well understood. The results showed agreement between the two systems to wavelengths as small as four times the diameter of the probe. One can calculate the transfer function associated with averaging a sine wave of wavelength λ over an interval L. The result is the familiar $\sin(x)/x$ function with $x = \pi L/\lambda$. This relation implies a half-power point (minus 3 db) at $\lambda = 2.25\ L$ and a minus 1 db point at $\lambda = 4L$. Siddon's result shows the

crossed wire and airfoil probe just starting to diverge at $\lambda = 4d$. The desired linear lift force due to the flow arises from the portion to the probe where the diameter changes and is in fact weighted by the rate of change of cross-sectional area. Thus the length over which the probe changes diameter rather than the diameter itself might be a more appropriate length scale. The change in area occurs in about 1.5 diameters for both of our probes and that described by Siddon (1969).

Crawford (1976) has analyzed the data collected with the Camel along the Atlantic Equatorial Undercurrent in order to study the energetics of the current. In the course of that work it was necessary to estimate the dissipation rates from the measured variance of the small-scale shears measured by the airfoil probe. As a check on the measured variances the velocity spectra were also computed by dividing out digitally, in the frequency domain of the spectra, the electronic time differentiation. The velocity spectra were fitted against a universal spectra for cross-stream fluctuations derived from the universal spectral shape for the downstream spectra of Nasmyth (1970). The fitting was done in the fashion described by Stewart and Grant (1962). Figure 16 shows the ratio of the estimated dissipation from fitting to the universal curve (ε_u) to the estimate from the measured variance (ε_m).

The relative shapes of the measured and universal spectra suggest that the probes have a poorer spatial resolution than the extrapolation of Siddon's results would lead one to expect. The minus 1 db point occurs at about 4 cm and the minus 3 db point at around 3 cm. These values suggest averaging length, L, of 1 cm and 1.3 cm, respectively, when used in the relations for the linear running average. These lengths are longer than the .75 cm over which the probe changes cross-sectional area or the .475 cm diameter. But this result is consistent with the wind tunnel results where the slope of the lift force curve increases and becomes non-linear as contributions from the straight section are included. The implication is clear that a shorter probe would be better and an optimum shape would include no cylindrical section, terminating the rubber just aft of the region of increasing radius.

It should be noted that errors in the probe sensitivities affect the accuracy of the curve fitting results. The ratio of the fits is linear in the sensitivities; the measured dissipation is quadratic and the dissipation calculated from the curve fit is cubic in the sensitivity. Also the validity of the curve fitting technique can be questioned since the data do not contain an extensive -5/3 region and may not represent isotropic turbulence with the energy containing eddies well separated in wave number space from the dissipation region.

One possible solution to determining the response of the probe is to simultaneously measure fluctuations with another cross-stream sensor, perhaps a laser doppler system. This measurement is an extremely difficult experimental problem in water. To some extent this comparison has already been made by Siddon, albeit in an air jet. The differences in his directly measured results and our derived results are a factor of 2 or 3 in size scale and that could well be due to the details of the different shapes.

An alternative approach to solving the problem of spatial resolution has been suggested by S Pond. It consists of making a probe that is small enough to allow confidence in resolving past the peak of the dissipation spectrum which is at $k \cong .14K_s$ (see Fig 17) for the cross-stream velocity component. Once past the peak of the dissipation spectrum it is reasonable to assume that $k^2\phi_{22}(k)$ vs. k is a self-similar function. Thus, the measured spectral shape can be extended in the reduced spatial response to obtain an estimate for the dissipation corrected for the probe response. This method was employed by Pond *et al.* (1966) on the downstream velocity component. So rather than fit the measured data against a universal spectral shape for velocity fluctuations the comparison is performed at higher wave numbers against a curve which is required to be monotonically decreasing with positive.

Figure 17 shows the dissipation spectra (derived by Crawford (1976) from the data of Nasmyth) for the cross-stream component in non-dimensional coordinates $k_s = (\varepsilon/\nu^3)^{\frac{1}{4}}$. If we require a probe to resolve to (i.e. be down 1 db or less) at $k/k_s = .3$. A maximum value for k_s can be estimated from a large value of $\varepsilon = 3 \times 10^{-2}$ cm^2/sec^3 and a small value for

$$\nu = .00918 \text{ cm}^2/\text{sec} \ (\theta=26°\text{C}).$$

$$k_s = \left(\frac{\varepsilon}{\nu^3}\right)^{\frac{1}{4}} = 14.03 \text{ cm}^{-1}$$

Resolution is desired to

$$k = .3\, k_s = 4.21 \text{ cm}^{-1}$$

The corresponding wavelength

$$\lambda = \frac{2\pi}{k} = 1.5 \text{ cm}$$

Our present probe is down 1 db at 4 cm so a probe 3/8 the present size with no straight section would be down 1 db at 1.5 cm. Needless to say, when a probe becomes this small it will be a single beam probe but that will have the advantage of more symmetric heating and cooling as well as simpler construction. Table 1 shows $\lambda = 2\pi/.3k$ and $\lambda = 2\pi/.25k_s$ the wavelength for 1 db depression in response as a function of ε and ν. A probe with a 2 cm averaging scale is good to $k = .3k_s$ if $\varepsilon < 10^{-2}$ or $\theta > 10°\text{C}$. At $k = .25k_s$ a 2 cm averaging probe would be limited to $\theta < 20°\text{C}$ or $\varepsilon < 2 \times 10^{-3}$ cm^2/sec^3. This table also shows an advantage to working in regions away from the Equator where the high temperature and concomitant low viscosities require better spatial resolution.

As a first step in using this method we plan to re-examine some of the Equatorial Undercurrent data as well as some of the Azores data by plotting the dissipation on linear-linear axes. An attempt is being made by A Nowell of the Institute of Ocean Sciences in Patricia Bay to ascertain the response of the present probes as a function of wave number by comparing a shear probe with the hot film probes in the far wake regime of a cylinder.

Conclusions

The airfoil probe is a very suitable and useful velocity sensor for oceanic turbulence studies. It has advantages over heated anemometry due to its rugged nature, lower susceptibility to fouling, and inherent linearity. Improvements are needed in the construction technique presently employed at UBC to make the probes. Work is in progress to simplify construction as well as to improve the characteristics with respect to the low-frequency thermal response. Measurements with the probe can be used to estimate the local rate of energy dissipation, which is a fundamental parameter that can be used to understand the energetics of oceanic currents. This approach was especially successful for Crawford (1976) in his work on the Atlantic Equatorial Undercurrent. From that work it is clear that the question of the spatial resolution of the oceanic probe is an important unsolved problem that needs investigation.

Acknowledgements

This work has been suppored by the National Research Council of Canada, the Department of Fisheries and the Environment, and the U S Office of Naval Research, on contract N00014-76-6-0446-NR083-207. This work has benefitted from many people who have given aid through the years. Dr P W Nasmyth first suggested the probe to one of the authors; Dr T E Siddon gave help, encouragement and information; Dr R W Stewart gave encouragement to the early work and Dr A E Gargett has been helpful in recent discussions. Dr Steve Pond gave very useful comments on an earlier draft; Dr G V Parkinson has helped with many discussions on aerodynamics. A special thanks to Dr A Nowell for showing some results, many useful discussions and comments on various points.

References

Abramovich, G N (1963) *The Theory of Turbulent Jets*. MIT Press, Cambridge, Mass.

Allen, H J and E W Perkins (1952) A study of effects of flow over slender inclined bodies of revolution. National Advisory Council for Aeronautics Report No 1048.

Bradshaw, P (1964) *Experimental Fluid Mechanics*. MacMillan, New York, 210 pp.

Bruce, J G and E J Katz (1976) Observations in the Equatorial Atlantic during GATE, June and July 1974 from ATLANTIS II. Woods Hole Oceanogr Inst Tech Rep 76-54 90 pp.

Crawford, W R (1976) Turbulent energy dissipation in the Atlantic Equatorial Undercurrent. PhD Thesis, University of British Columbia. 145 pp.

Grant, H L, R W Stewart and A Moilliet (1962) Turbulence spectra from a tidal channel. J Fluid Mech *12*: 241-263.

Lamb, H (1945) *Hydrodynamics*. Sixth Edition. Dover Publications. 738 pp.

Lock, C N H and F C Johansen (1931) Wind tunnel interference on streamline bodies; theory and experiments. Aeronautical Research Committee Reports and Memoranda No 1451.

Lumley, J L and J F McMahon (1976) Reducing water tunnel turbulence by means of a honeycomb. Trans of the ASME, paper no 67-fe-5.

Nasmyth, P W (1970) Oceanic Turbulence. PhD Thesis, Inst of Oceanography, University of British Columbia.

Nielsen, J N (1960) *Missile Aerodynamics*. McGraw-Hill, New York. 450 pp.

Oakey, N S (1977) An Instrument to Measure Oceanic Turbulence and Microstructure. Bedford Institute of Oceanography Report Series/BI-R-77-3/ May 1977.

Osborn, T R (1974) Vertical profiling of velocity microstructure. J Phys Oceanogr *4*: 109-115.

Osborn, T R and T E Siddon (1975) Oceanic shear measurements using the airfoil probe. Proceedings Third Biennial Symposium on Turbulence in Liquids, Rolla, Missouri.

Pankhurst, R C and D W Holder (1952) *Wind-Tunnel Technique*. Pitman, London. 702 pp.

Pond, S, S D Smith, P F Hamblin, and R W Burling (1966) Spectra of velocity and temperature fluctuations in the atmospheric boundary layer over the sea. J Atmos Sci *23*: 376.

Siddon, T E (1965) A turbulence probe utilizing aerodynamic lift. University of Toronto, Inst for Aerospace Studies. Tech Note 88.

Siddon, T E (1969) On the response of pressure measuring instrumentation in unsteady flow. University of Toronto, Inst for Aerospace Studies, Report No 136.

Siddon, T E (1971) A minature turbulence gauge utilizing aerodynamic lift. Rev Sci Inst, *42*: 653-656.

Siddon, T E (1974) A new type turbulence gauge for use in liquids. Proceedings of 1971 Symposium on Flow - its measurement and control in science and industry. Pittsburgh. Proceedings published 1974. 435-439

Siddon, T E and H S Ribner (1965) An aerofoil probe for measuring the transverse component of turbulence. AIAAJ. Apr 1965, 747-749.

Smith, R H and C Wang (1944) Contracting cones giving uniform throat speeds. J of the Aeronautical Sci 11 356-360.

von Kármán, Th and W R Sears (1938) Airfoil Theory for Non-Uniform Motion. J Aeronautical Sciences, Vol 5, No 10, pp 379-390.

TABLE I

		ε	$3\times10^{-2}\frac{am^2}{sec^3}$	10^{-2}
θ	ν			
26°C	.00918		1.5 (1.8)	2.0 (2.4)
20°C	.0105		1.7 (2.0)	2.2 (2.6)
15°C	.0120		1.8 (2.2)	2.4 (2.9)
10°C	.0136		2.0 (2.4)	2.6 (3.2)

$\lambda = 2\Pi/k$ where $k = .3k_s$ and $.25\ k_s$ in parenthesis.

List of Figures

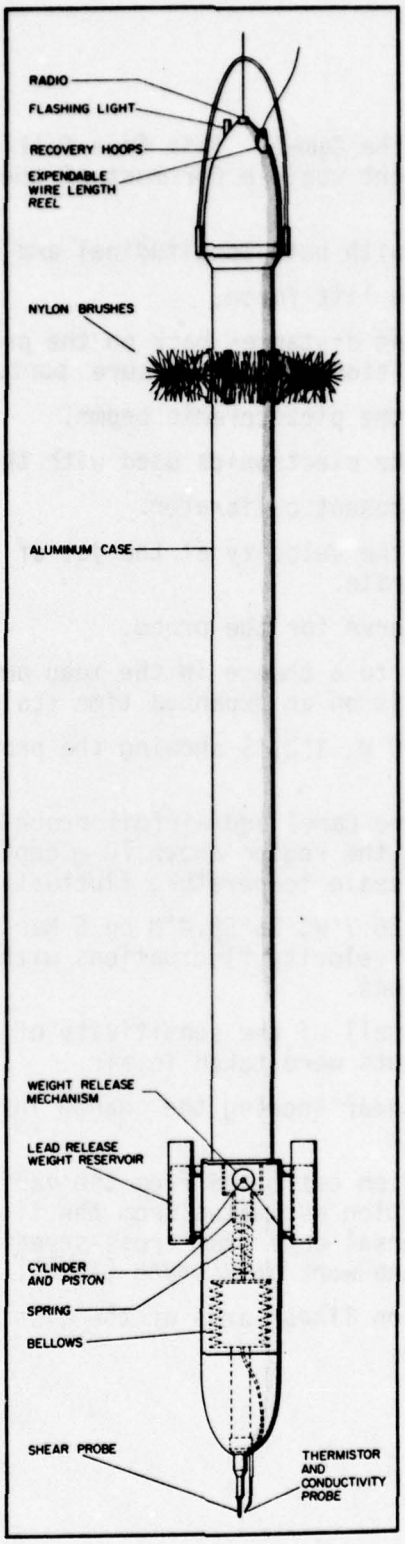
RADIO
FLASHING LIGHT
RECOVERY HOOPS
EXPENDABLE WIRE LENGTH REEL
NYLON BRUSHES
ALUMINUM CASE
WEIGHT RELEASE MECHANISM
LEAD RELEASE WEIGHT RESERVOIR
CYLINDER AND PISTON
SPRING
BELLOWS
SHEAR PROBE
THERMISTOR AND CONDUCTIVITY PROBE

Figure 1

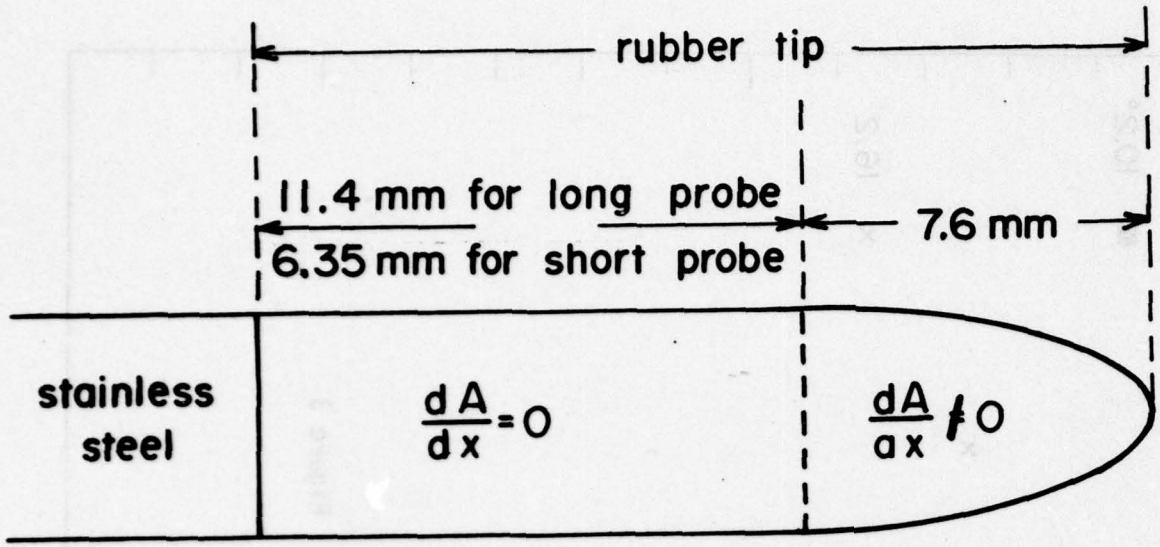

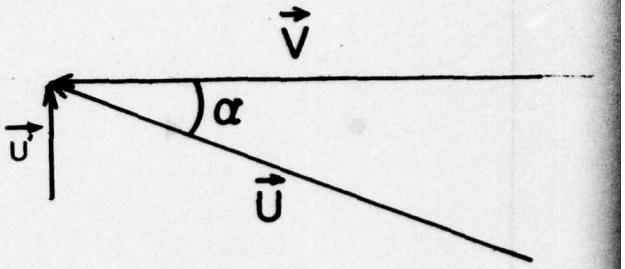

$$\vec{U} = \vec{V} + \vec{u}$$

END VIEW

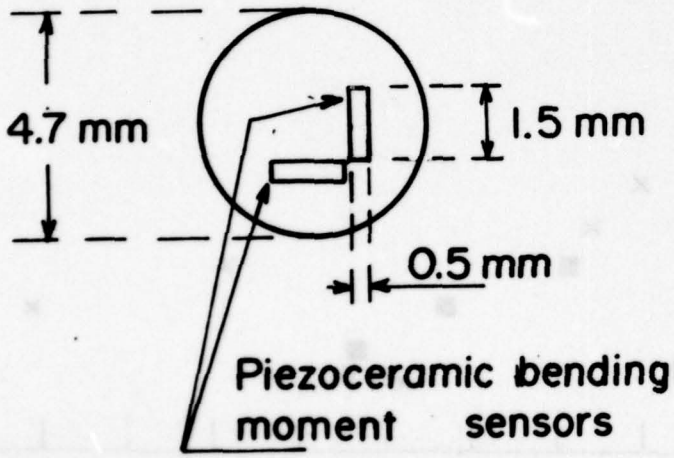

Figure 2

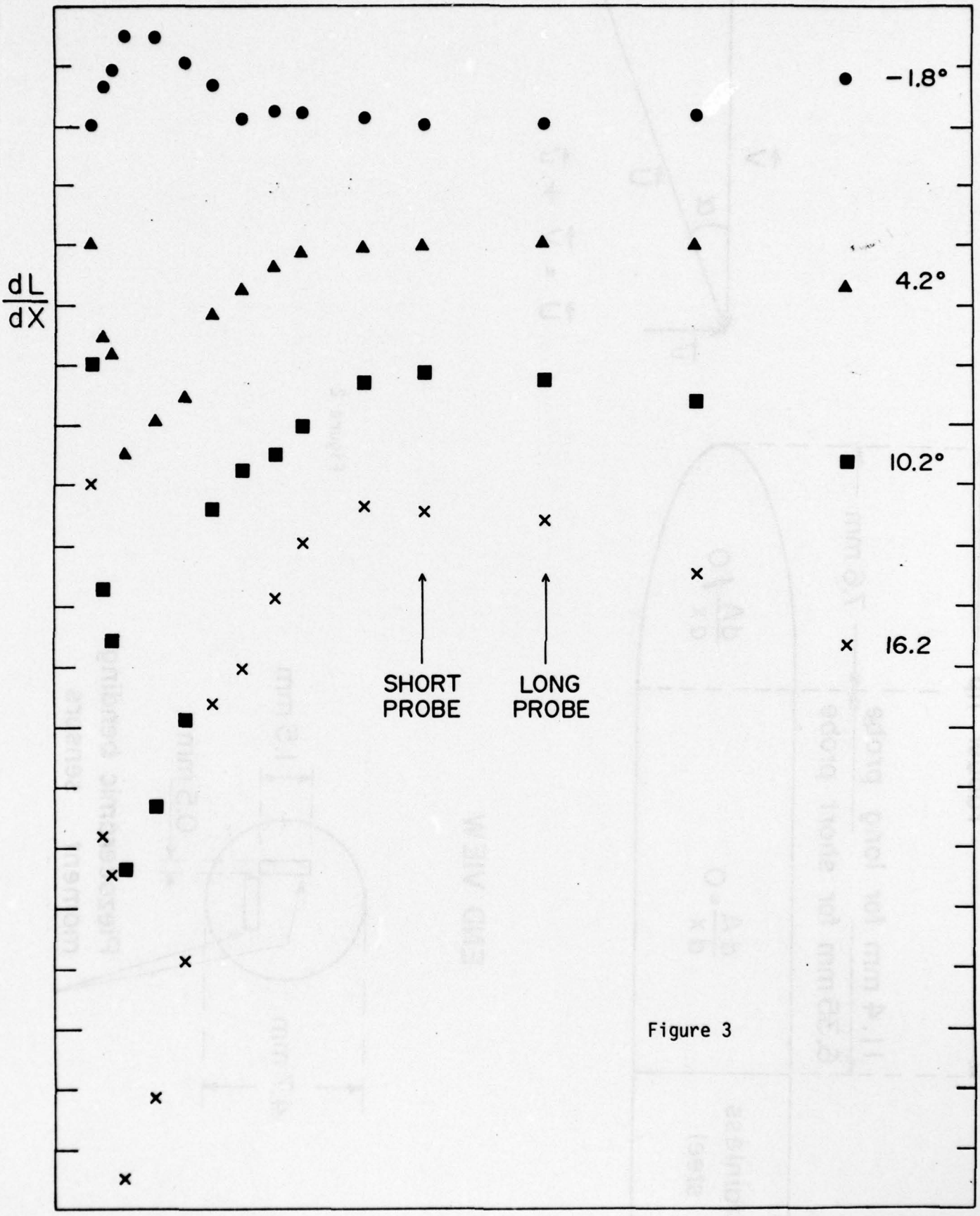

Figure 3

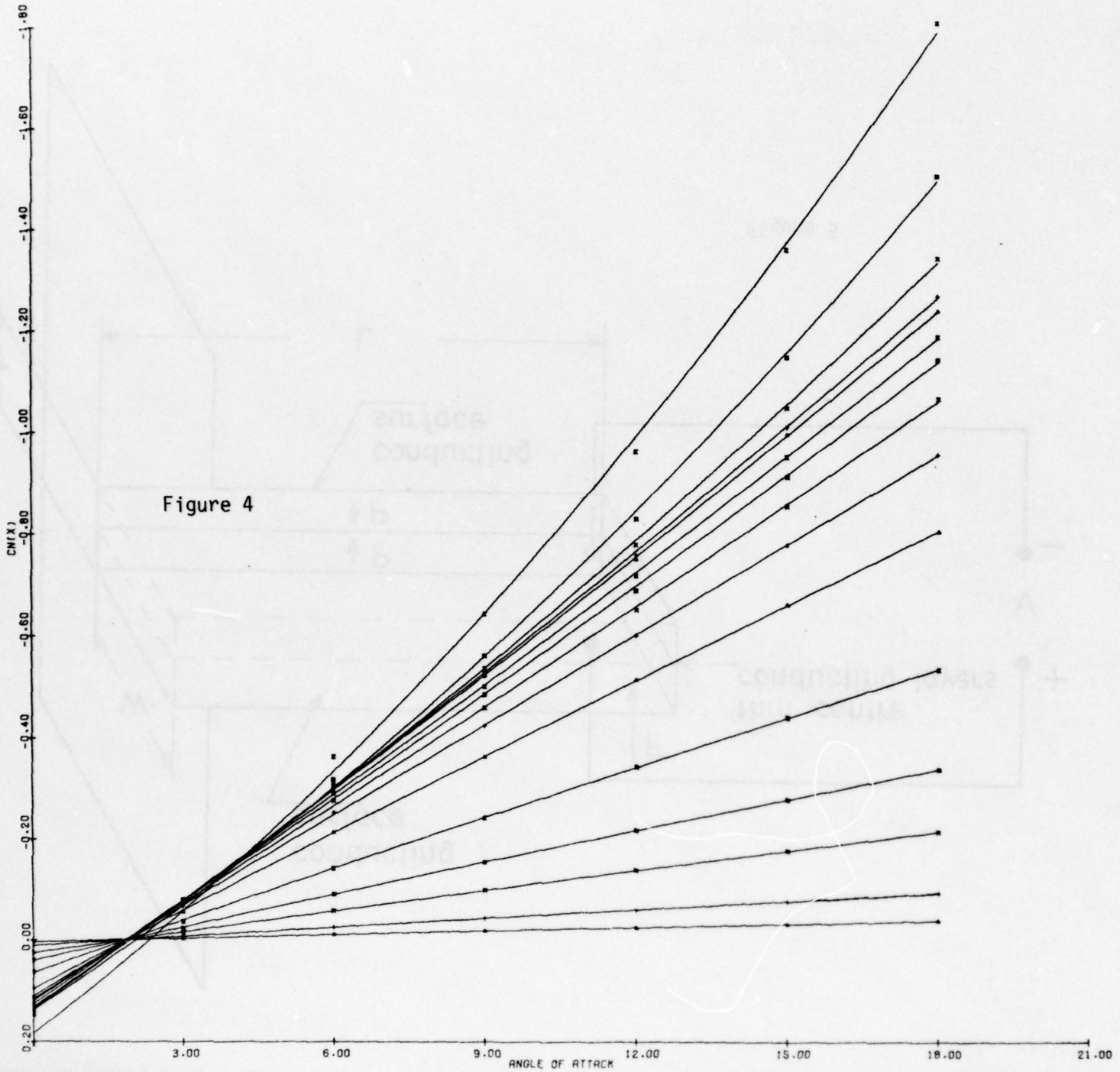
CN(X)
-1.80
-1.60
-1.40
-1.20
-1.00
-0.80
-0.60
-0.40
-0.20
0.00
0.20
3.00
6.00
9.00
12.00
15.00
18.00
21.00
ANGLE OF ATTACK

Figure 4

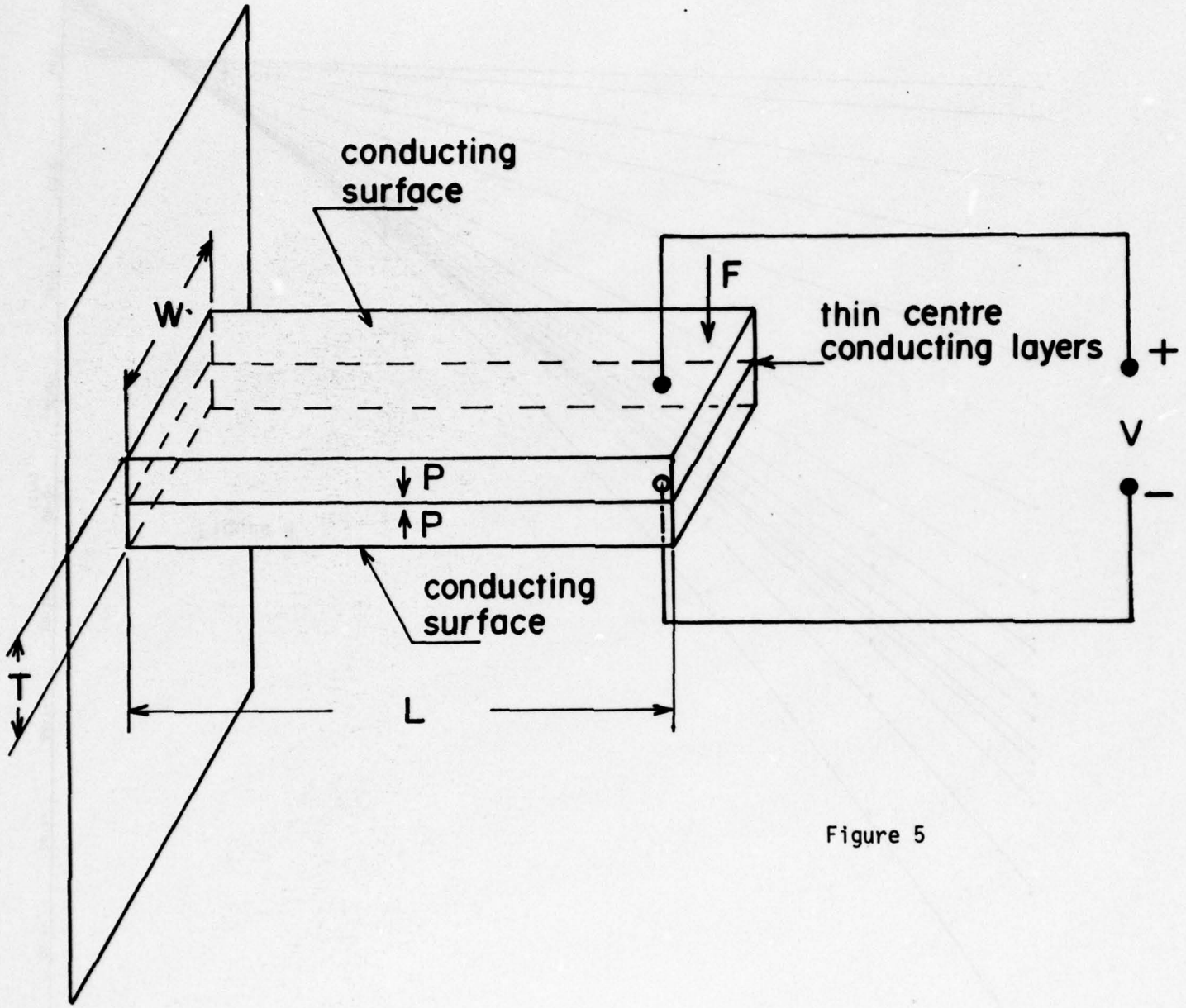
conducting
surface
W
F
thin centre
conducting layers
+
V
−
P
P
conducting
surface
T
L

Figure 5

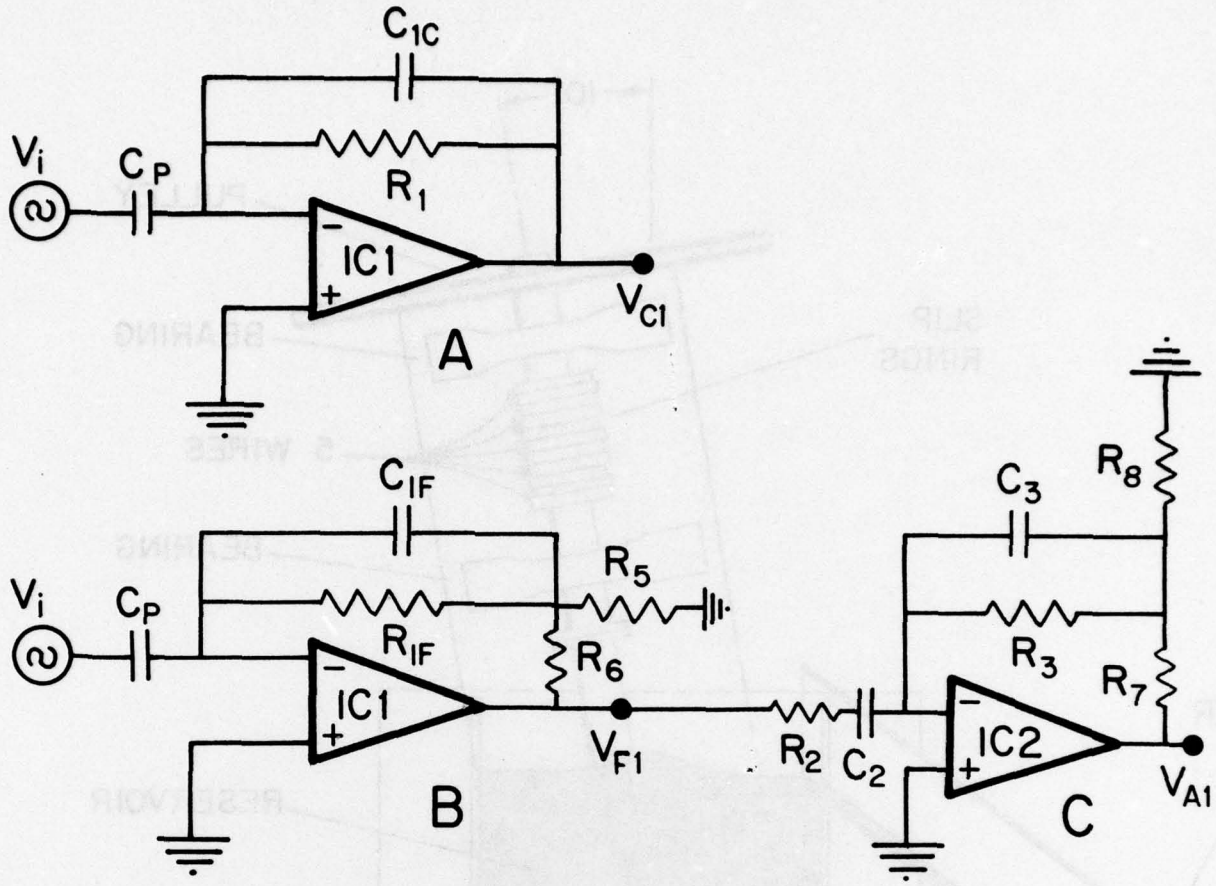

A Calibration preamplifier
B Differentiating field preamplifier
C Amplifier

C_{1c}	1.5×10^{-10} f	R_1	$10^{10}\ \Omega$	R_7	$1. \times 10^{4}\ \Omega$
C_{1F}	1.3×10^{-10} f	R_{1F}	$2.2 \times 10^{7}\ \Omega$	R_8	$1.9 \times 10^{2}\ \Omega$
C_2	$1. \times 10^{-6}$ f	R_2	$1.7 \times 10^{5}\ \Omega$		
C_3	1.5×10^{-8} f	R_3	$1.6 \times 10^{5}\ \Omega$		
IC1	AD503K	R_5	$1. \times 10^{3}\ \Omega$		
IC2	A777	R_6	$1. \times 10^{4}\ \Omega$		

Figure 6

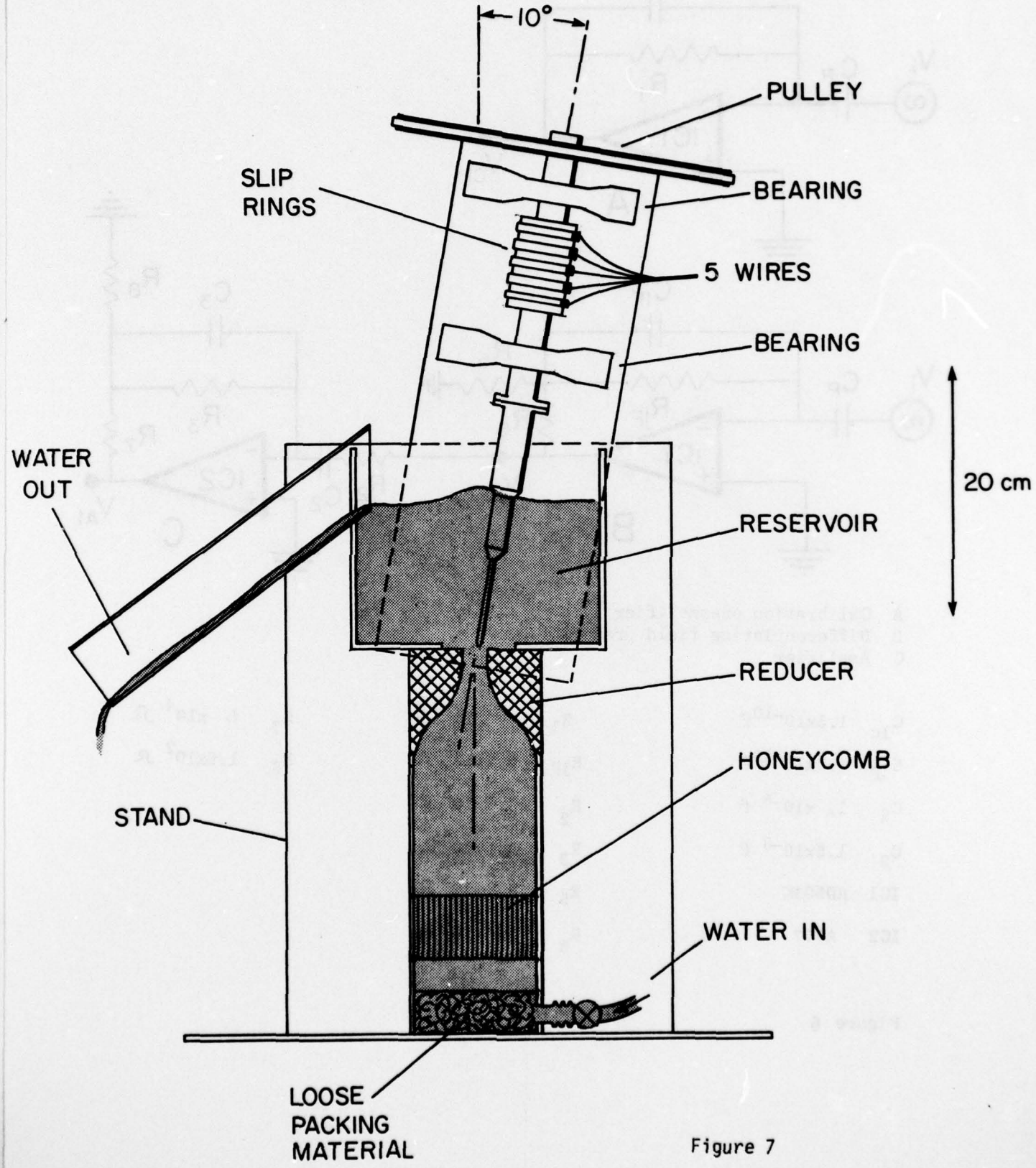
10°
PULLEY
SLIP RINGS
BEARING
5 WIRES
BEARING
WATER OUT
20 cm
RESERVOIR
REDUCER
HONEYCOMB
STAND
WATER IN
LOOSE PACKING MATERIAL

Figure 7

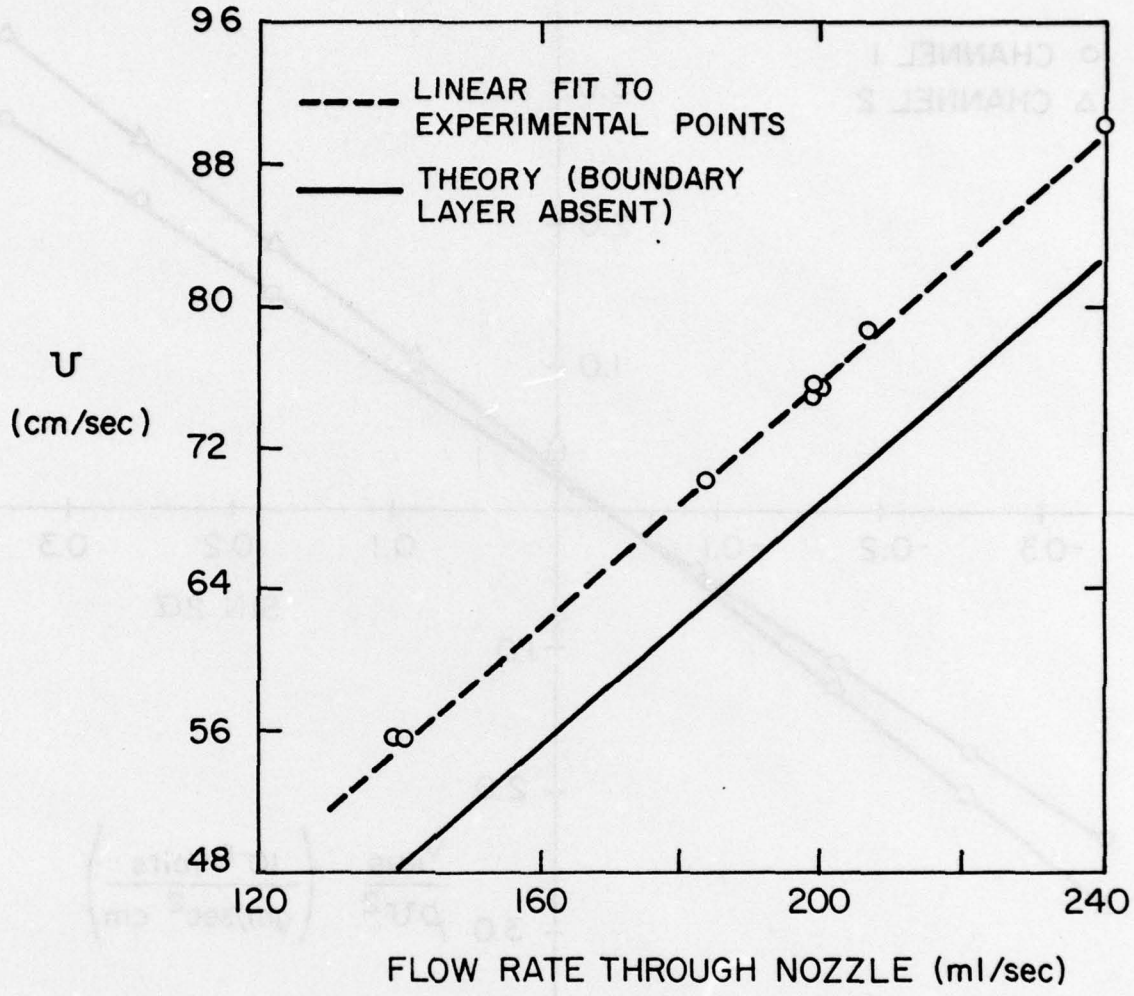
96
88
80
72
64
56
48
U
(cm/sec)
LINEAR FIT TO
EXPERIMENTAL POINTS
THEORY (BOUNDARY
LAYER ABSENT)
120
160
200
240
FLOW RATE THROUGH NOZZLE (ml/sec)

Figure 8

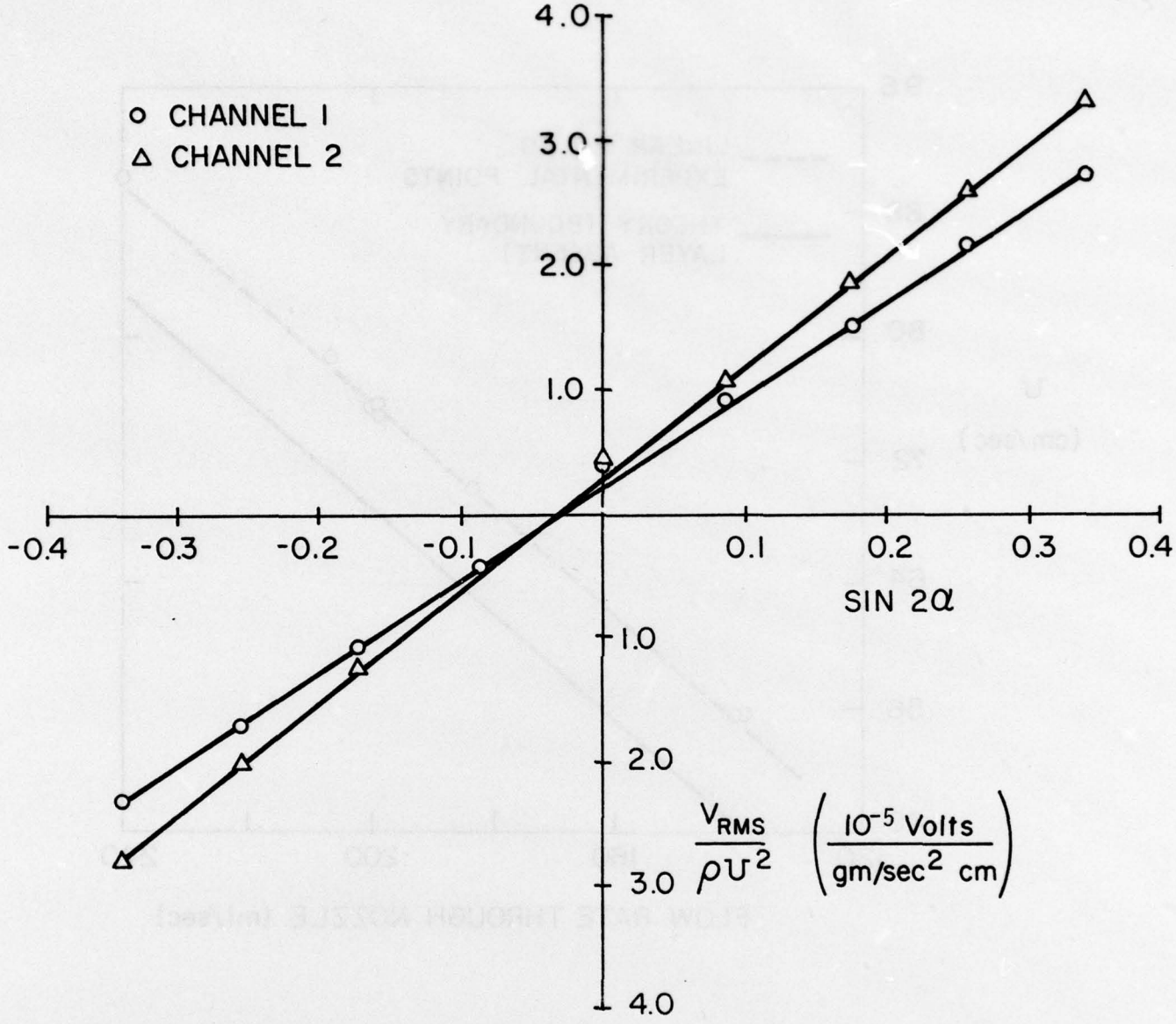
CHANNEL 1
CHANNEL 2
4.0
3.0
2.0
1.0
-0.4
-0.3
-0.2
-0.1
0.1
0.2
0.3
0.4
SIN 2α
1.0
2.0
3.0
4.0
$\frac{V_{RMS}}{\rho U^2}$ $\left(\frac{10^{-5}\ \text{Volts}}{\text{gm/sec}^2\ \text{cm}}\right)$

Figure 9

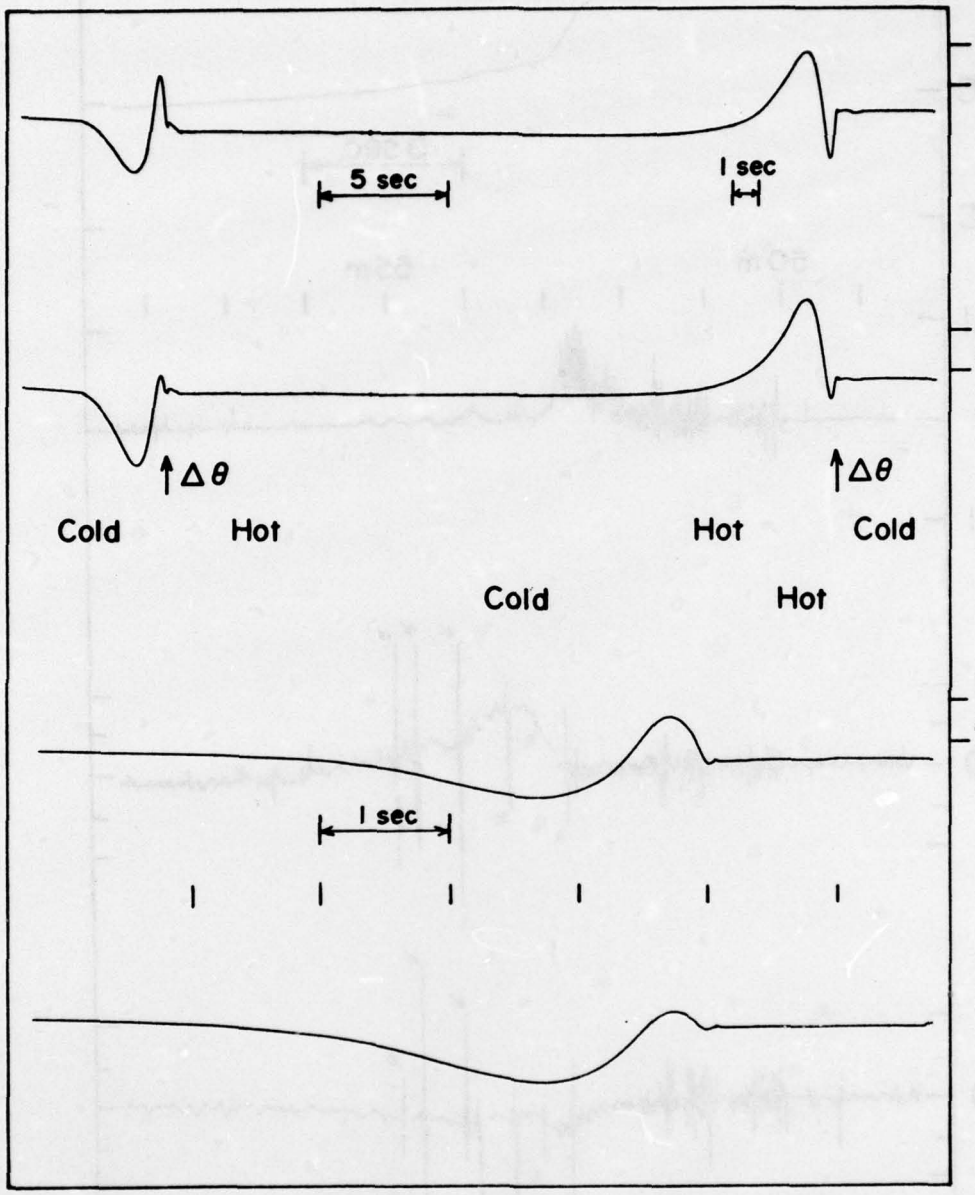
ΔV = 1 volt
5 sec
1 sec
(10a)
ΔV = 1 volt
Δθ
Δθ
Cold
Hot
Hot
Cold
Cold
Hot
ΔV = 1 volt
1 sec
(10b)

Figure 10

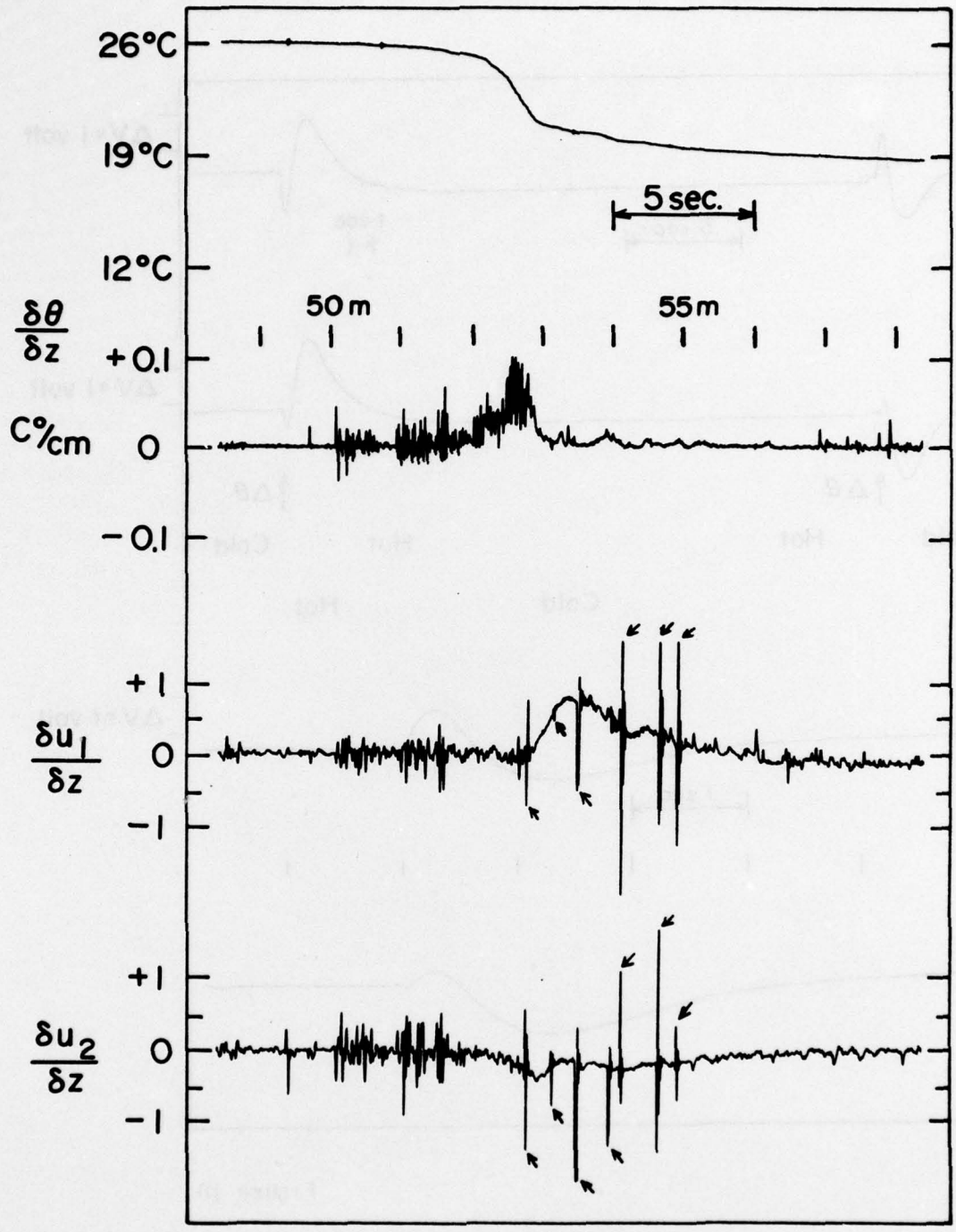

Figure 11

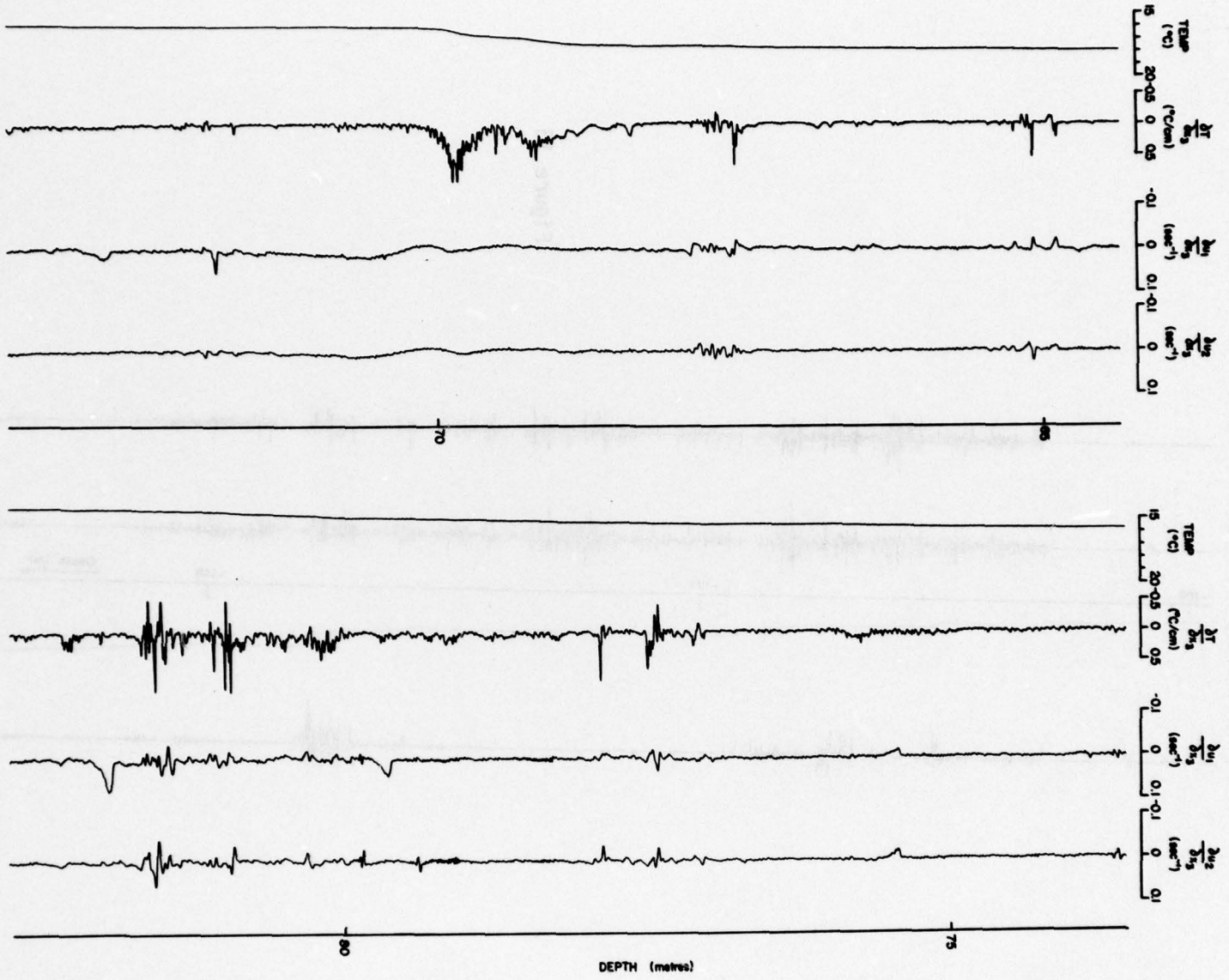

Figure 12

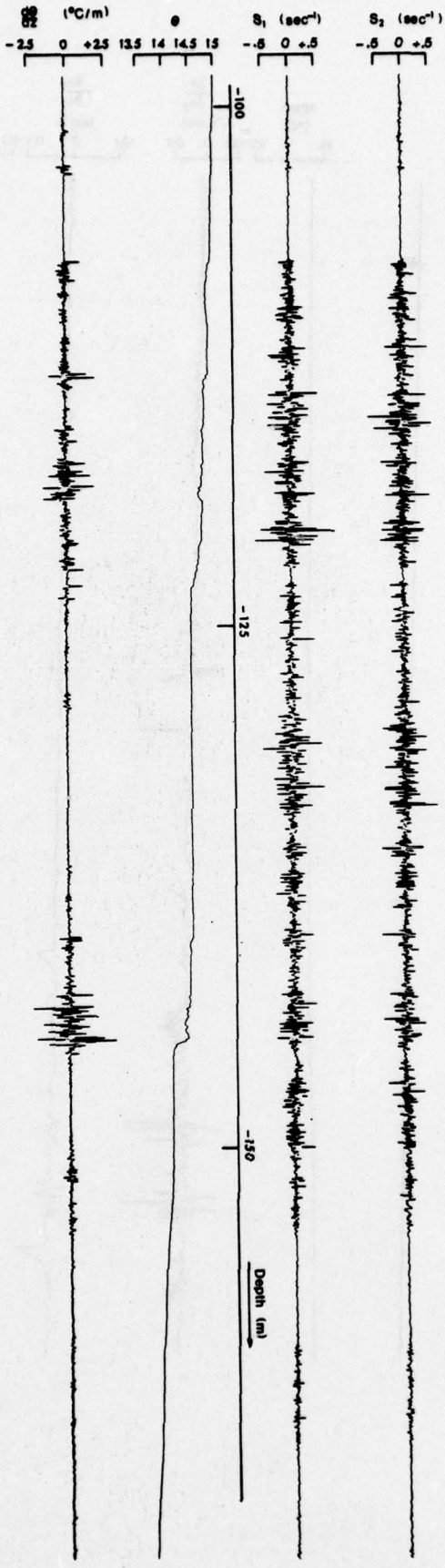
DROP 6
(°C/m)
-2.5 0 +2.5
θ
13.5 14 14.5 15
S1 (sec-1)
-.5 0 +.5
S2 (sec-1)
-.5 0 +.5
-100
-125
-150
Depth (m)

Figure 13

Figure 14

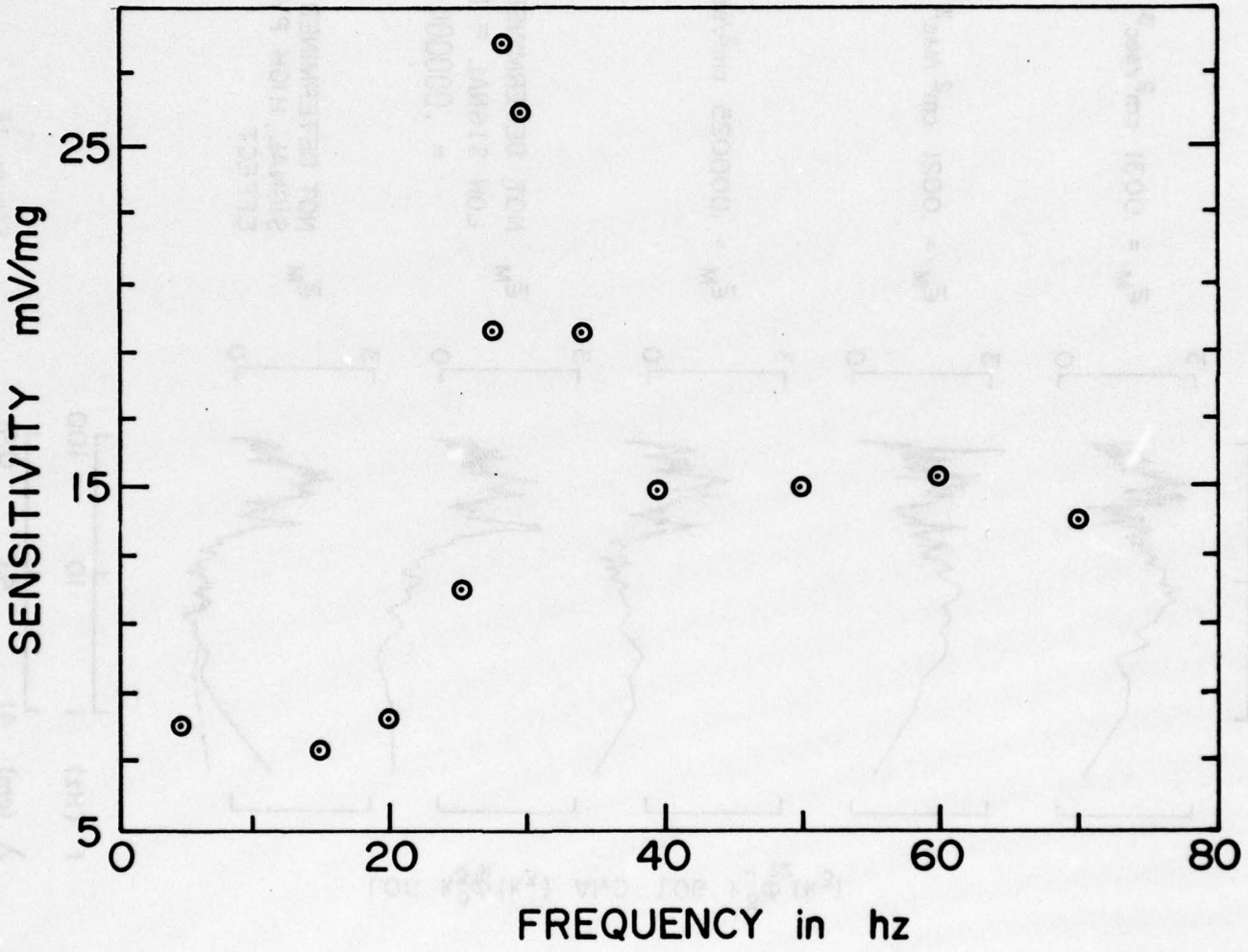

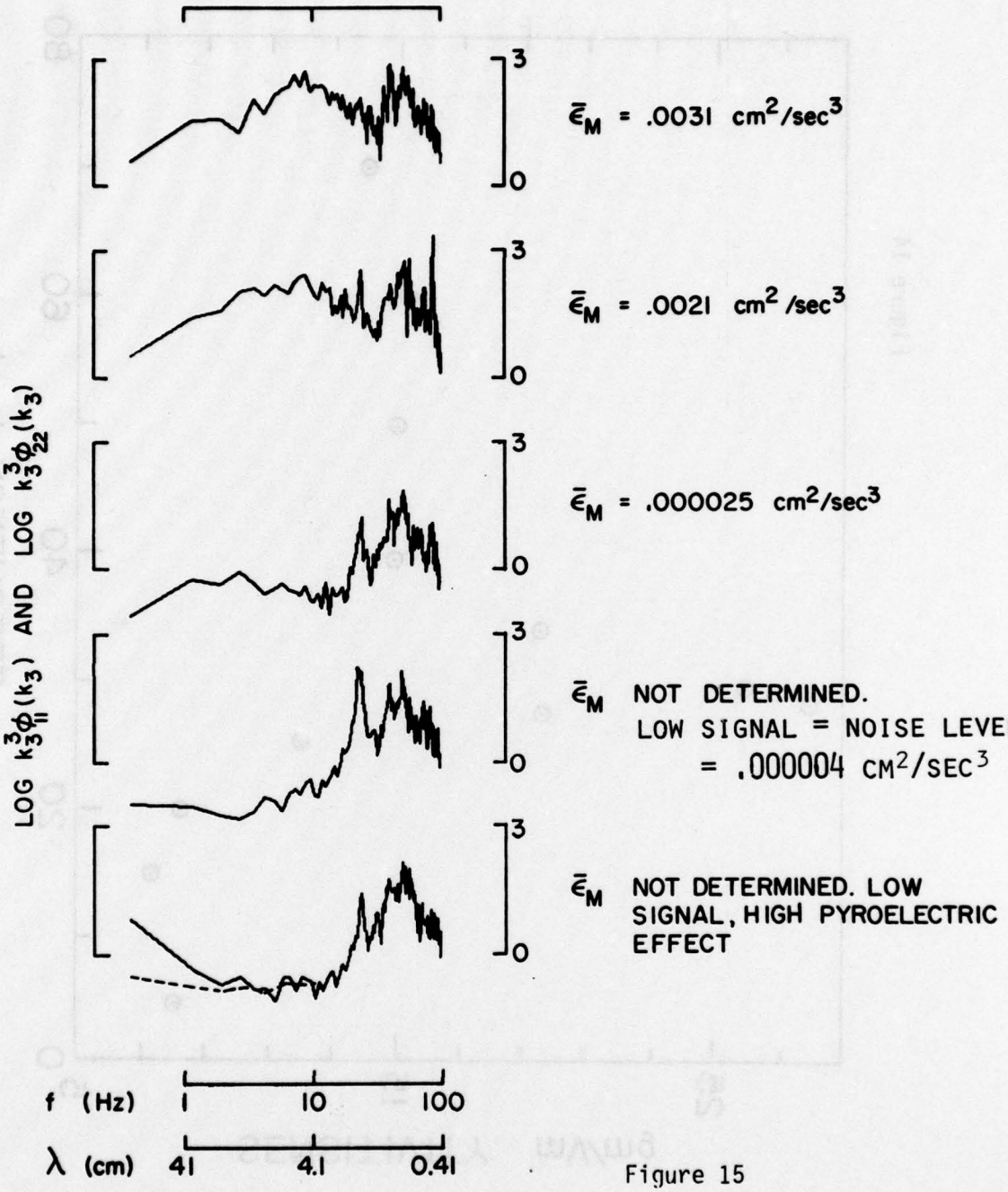
LOG $k_3^3\phi_{11}(k_3)$ AND LOG $k_3^3\phi_{22}(k_3)$
3
0
$\bar{\epsilon}_M$ = .0031 cm²/sec³
$\bar{\epsilon}_M$ = .0021 cm²/sec³
$\bar{\epsilon}_M$ = .000025 cm²/sec³
$\bar{\epsilon}_M$ NOT DETERMINED.
LOW SIGNAL = NOISE LEVEL
= .000004 CM²/SEC³
$\bar{\epsilon}_M$ NOT DETERMINED. LOW SIGNAL, HIGH PYROELECTRIC EFFECT
f (Hz) 1 10 100
λ (cm) 41 4.1 0.41

Figure 15

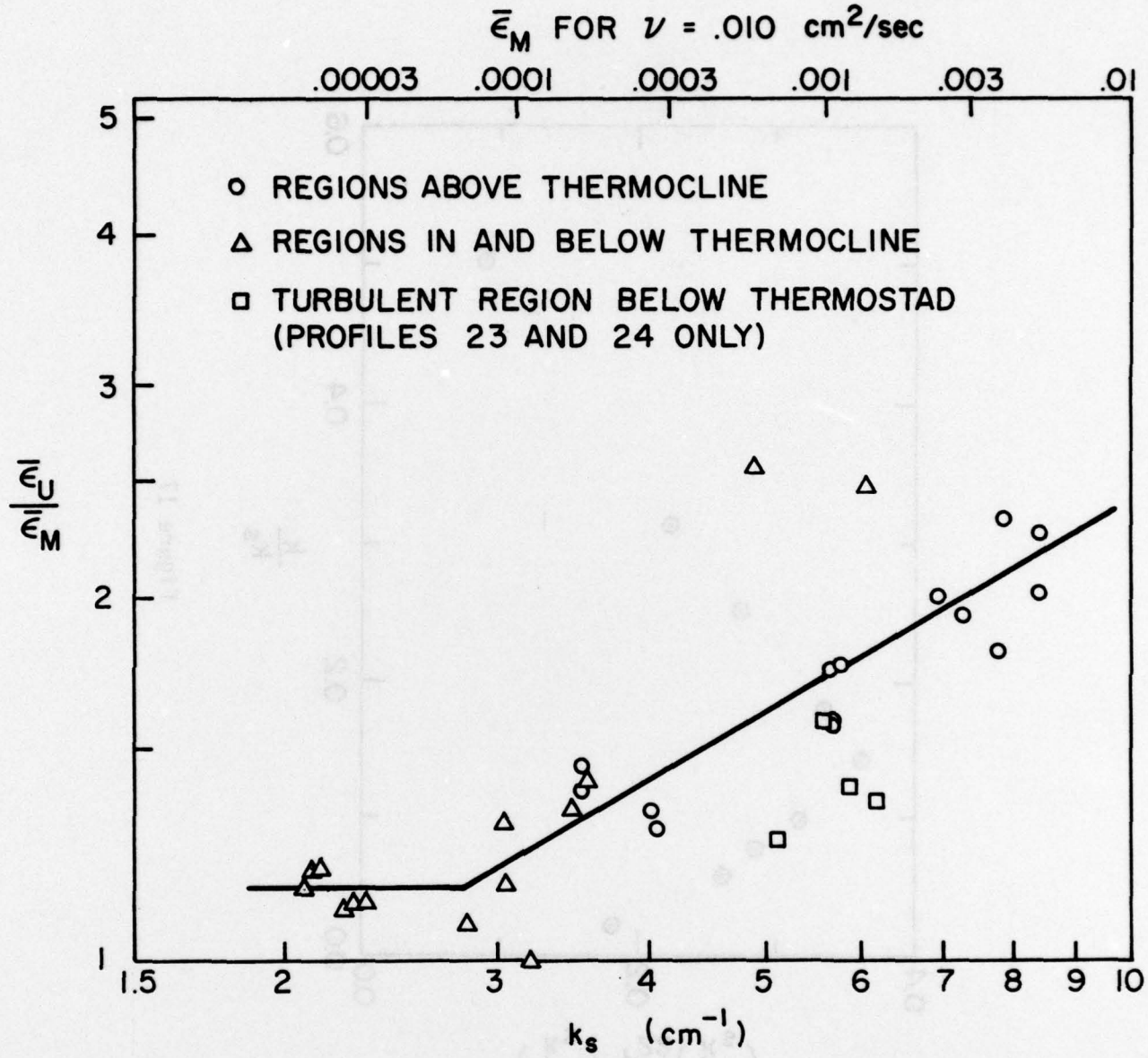
$\bar{\epsilon}_M$ FOR ν = .010 cm^2/sec
.00003
.0001
.0003
.001
.003
.01
REGIONS ABOVE THERMOCLINE
REGIONS IN AND BELOW THERMOCLINE
TURBULENT REGION BELOW THERMOSTAD
(PROFILES 23 AND 24 ONLY)
$\frac{\bar{\epsilon}_U}{\bar{\epsilon}_M}$
1
2
3
4
5
1.5
2
3
4
5
6
7
8
9
10
k_s (cm^{-1})

Figure 16

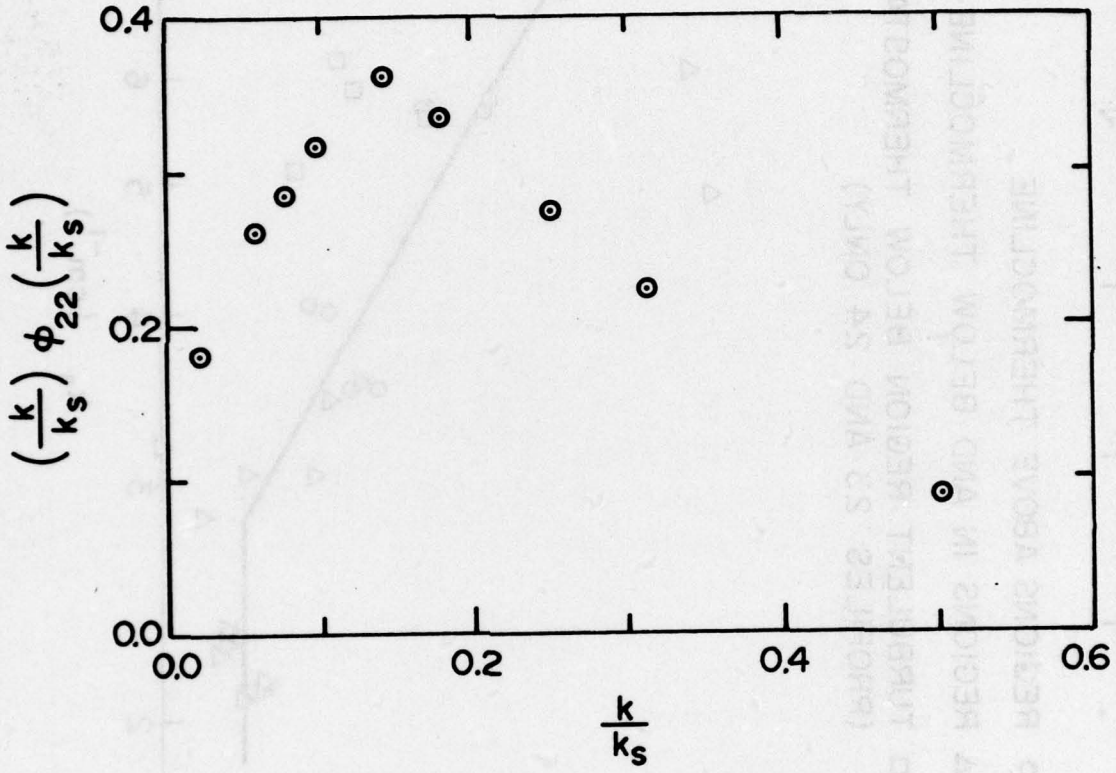
0.4
0.2
0.0
0.0
0.2
0.4
0.6
$\left(\frac{k}{k_s}\right) \Phi_{22}\left(\frac{k}{k_s}\right)$
$\frac{k}{k_s}$

Figure 17